

Section 5

Development of and studies with regional and smaller-scale atmospheric models, regional ensemble, monthly and seasonal forecasting

The new very short range forecast model COSMO-LMK for the convection-resolving scale

M. Baldauf, K. Stephan, S. Klink, C. Schraff, A. Seifert, J. Förstner, T. Reinhardt, C.-J. Lenz
Deutscher Wetterdienst, Kaiserleistr. 42, 63067 Offenbach, Germany
e-mail: michael.baldauf@dwd.de

1. Introduction

Up to now the model chain of the Deutscher Wetterdienst (German Weather Service, DWD) is built up by the global model GME with about 40 km resolution and the regional, meso-beta model LME (commonly developed in COSMO, <http://www.cosmo-model.org>) with 7 km resolution. Since August 2006, the newly developed numerical weather prediction system LMK ('LM-Kürzestfrist') for very short range forecasts (up to 18h) and with a resolution on the meso-gamma scale ($dx=2.8\text{km}$) is in a pre-operational trial at the DWD. This is the first time that a convection resolving model is used at the DWD. The emphasis of this model system lies in the prediction of severe weather events related to deep moist convection and to interactions of the flow with small scale topography.

The currently used LMK-configuration covers the domains of Germany, Switzerland and Austria and smaller parts of the other neighbouring countries with $421 \times 461 \times 50$ gridpoints and a horizontal resolution of 2.8 km.

The project LMK was established at the DWD in the mid of 2003 within the scope of the 'Aktionsprogramm 2003' and ended in December 2006. It was subdivided into four sub-projects:

1. Supply of quality controlled radar-precipitation data.
2. The installation of an assimilation method for radar reflectivity using latent heat nudging to provide highly resolved initial fields, especially for the initiation of convection.
3. The advancement of the numerical model based on the currently used LM.
4. Finally the accompanying verification and the advancement of verification methods for horizontal model resolutions of about 2.8 km.

2. Latent heat nudging

A meso- γ -model has special requirements concerning data assimilation: at this scale highly resolved, rapidly updated data fields are needed, which can in principle be delivered by radar observations. The German radar network has a spatial resolution of radially 1 km and laterally 1° and a temporal resolution of 5 min. for the precipitation scan. The assimilation method should be fast and also relatively easy to implement. The latent heat nudging (LHN) approach fulfills these requirements. It uses the differences between (radar) measured and simulated precipitation rates and interpretes them

as a lack or surplus of latent heat along the trajectory of a condensed particle. One basic assumption of the LHN is that this relation is valid in a vertical model column. This basic assumption stands in contradiction to the use of a prognostic precipitation scheme which drifts rain and snow by several grid lengths over several time steps. This leads to some sort of feedback problem, which can be solved partially by using an undelayed reference precipitation step additionally to the prognostic precipitation step. Another improvement can be obtained by using latent heating increments only in the growth stage of a convective cell. These modifications led to a more realistic assimilation of the precipitation pattern of convective events (Schraff et al. (2006)).

3. Numerical model development

The dynamical formulation of the LMK bases on the COSMO-Lokal Modell (LM) (Doms and Schättler (2002)): it is a non-hydrostatic, fully compressible model in advection form. But there are some differences in the numerical formulation. LMK now uses a two-timelevel integration scheme based on the Runge-Kutta-method of 3. order for the prediction of the 3 cartesian wind components u, v, w , the pressure perturbation p' from a hydrostatic base state, and the temperature perturbation T' . This allows the use of an upwind advection scheme of 5. order in the horizontal with Courant-numbers up to 1.4 (Wicker and Skamarock (2002)). For the 6 humidity variables (mass fractions of water vapour, cloud and rain water, cloud ice, snow and graupel) several Courant-number-independent Euler- and Semi-Lagrange-schemes can be used (Förstner et al. (2006)). Idealised tests of this new dynamical core with linear mountain flow and nonlinear density current simulations performed very well.

One of the most farreaching changes from LM is that LMK will not longer use a deep convection parameterisation. Instead of this, LMK aims to resolve moist convection explicitly. For the smaller scales of convection the slightly modified shallow convection scheme of the Tiedtke Cumulus parameterization scheme is used. This parameterization especially takes care of the transport of moisture from the boundary layer to a height of about 3 km and therefore avoids the overestimation of low cloud coverage. Without a deep convection parameterization the need for a faster sedimenting ice phase seems to be necessary. Therefore the former 5-class microphysics scheme was extended by a new precipitation class 'graupel'. This new scheme was tested with the IMPROVE-2 data set and one day of the BAMEX field campaign. In

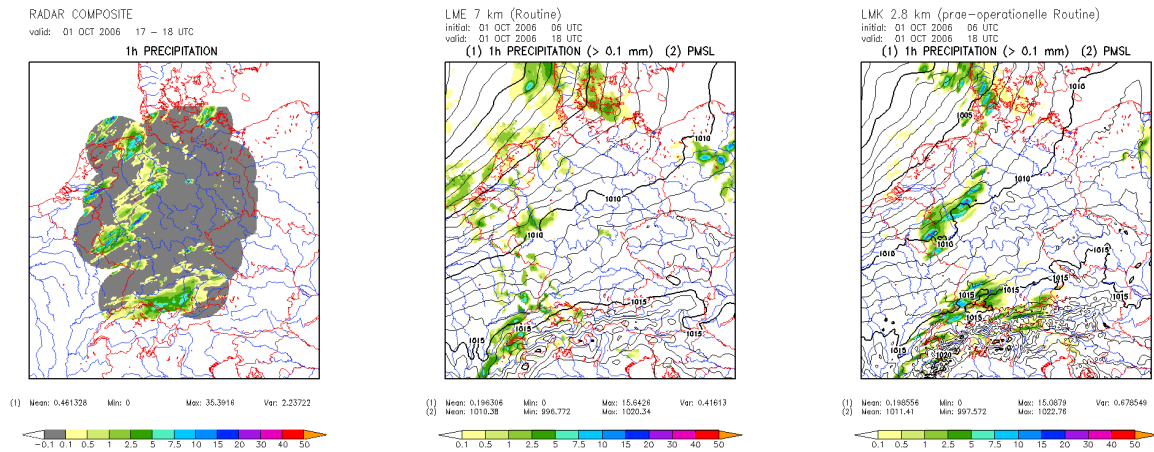


Figure 1: Radar observation (left), LME- (middle), and LMK- (right) simulations of convectively amplified frontal precipitation at 01.10.2006

the latter test case, the ability of the LM to resolve deep convection could also be shown. Further improvements of the physics packages are the introduction of 3-dimensional turbulence with full metrics (Baldauf (2006)) (but which is not used up to now in the pre-operational runs) and a new 7-layer soil model. For the problem of underestimation of precipitation in convective situations, the resolution of 2.8 km is not responsible, as could be shown by comparisons with 1km runs. Instead this problem could be cured by reducing the evaporation of rain below the cloud base and by making changes in the boundary layer parameterisation of subgrid scale clouds.

4. Experiences from the pre-operational test phase

In general, LMK has better scores for wind speed and gusts in 10 m above ground. The RMSE of the wind speed is reduced by about 5 to 10 % compared to LME. The RMSE of 2m temperature is mostly smaller in LMK, too, although no soil moisture analysis is used. The precipitation forecast had better true skill statistics (TSS) in the months September to November 2006. But in December, LMK had drawbacks compared to LME. This is partly due to the fact, that LHN is switched off in winter months due to bright bands in the radar data, which are up to now not corrected. The stratification of LMK is often slightly too unstable, which gives the hint, that convection is not efficiently enough resolved by the model. In contrary, LME produces too stable stratifications, an artefact of the parameterization.

The figures show an example ('01.10.2007'), where frontal precipitation is convectively increased. Whereas the parameterisation of LME does not initiate convection in western

Germany, LMK is able to reproduce at least a bigger part of the rain area at the correct time, compared to radar observations.

In general LMK improves precipitation forecasts in situations, where convection is connected with a synoptic forcing, whereas it does not perform as well in free convection situations. Here, only the latent heat nudging can trigger precipitation events a few hours in advance.

LMK has clear advantages in more dynamically driven phenomena due to its better spatial resolution. Lee waves are often correctly forecasted, which gives an increased skill for aviation, especially for gliders. Strong downslope winds in stably stratified atmosphere are better forecasted too, an example was found at 05.11.2006 in the lee of the Erzgebirge, where a hydraulic jump could be simulated by LMK.

The operational usage is planned for April 2007.

References

- Baldauf, M (2006): Implementation of the 3D-Turbulence Metric Terms in LMK, *COSMO-Newsletter*, 6:44–50.
- Doms, G. and U. Schättler (2002): A Description of the Non-hydrostatic Regional Model LM, *Deutscher Wetterdienst*, Nov. 2002.
- Förstner, J., M. Baldauf and A. Seifert (2006): Courant Number Independent Advection of the Moisture Quantities for the LMK. *COSMO-Newsletter*, 6: 51–64.
- Wicker, L.J. and W.C. Skamarock (2002): Time splitting methods for elastic models using forward time schemes. *Mon. Wea. Rev.*, 130, 2088–2097.
- Schraff, C., K. Stephan, and S. Klink (2006): Revised Latent Heat Nudging to cope with Prognostic Precipitation. *COSMO-Newsletter*, 6:31–37, 2006.

Surface wind prediction by the boundary layer model

L. Berkovich, Yu. Tkacheva (berkovich@mecom.ru)

Russian Hydro-meteorological Research Centre, Moscow

V. Shnaydman

New Jersey State University-Rutgers, New Brunswick, New Jersey

The reliable surface wind prediction plays an important role in the meteorological service of the atmospheric pollution, take off and landing of the airplanes.

The most of operational schemes of surface wind prediction apply the models of surface layer based on the Monin-Obukhov similarity theory which uses the set of constrictions and empirical formulas. It reduces the quality of the forecasts.

The distinguishing feature of the approach used in Russian Hydro-meteorological Center (RHMC) is refusal of the surface layer separation and spreading the algorithm of the advanced atmospheric boundary layer (ABL) model (Shnaydman and Berkovich) to entire calculation area from the underlying surface to the top of ABL with the lower no-slip vertical condition on the level of roughness. It allowed to calculate the characteristics of the surface layer by taking into account the main physical mechanisms of space distribution of turbulence parameters and meteorological variables including the surface wind on the level of 10m.

The prediction of the surface wind was carried out by Forecasting System of RHMC which combine the scheme of forecasting the large scale atmospheric processes and the ABL formation. Here it was shown the results of near surface transfer reconstruction for the Europe, where the dense meteorological network and advanced ABL model gave the possibility of wind reconstruction with the good comparison of the predictions and objective analysis (OA) data. The comparisons done (non published results) showed that the wind measurements and OA data were close if the forecasting scheme had the horizontal resolution by the order of mean distance between the meteorological stations.

The brief description of the transfer near the underlying surface for Europe is given for 00 UTC 12 April 2005. The main peculiarities of the near surface transfer were the flows from west to east in the belt 70-75N, from south and south-west to north and north-east from 52-70N one. The wind between the lines connecting the points 57N and 70N at the west boundary, 42N and 59N at the east boundary got 12m/s. This zone was the most evidently expressed during the initial 12 hours. Then it weakened and shifted to the north as far as the prediction period increased to 36 hours.

The comparisons of the predictions and OA data were given by the mapping of the module and direction surface winds, the table of errors and the correlation coefficients. The predicted fields of surface wind represented the main straits of actual horizontal distributions of the module and direction of the near surface transfer. The predicted wind directions were in good agreement with the OA data especially in the areas where the wind speed is more than 2m/s.

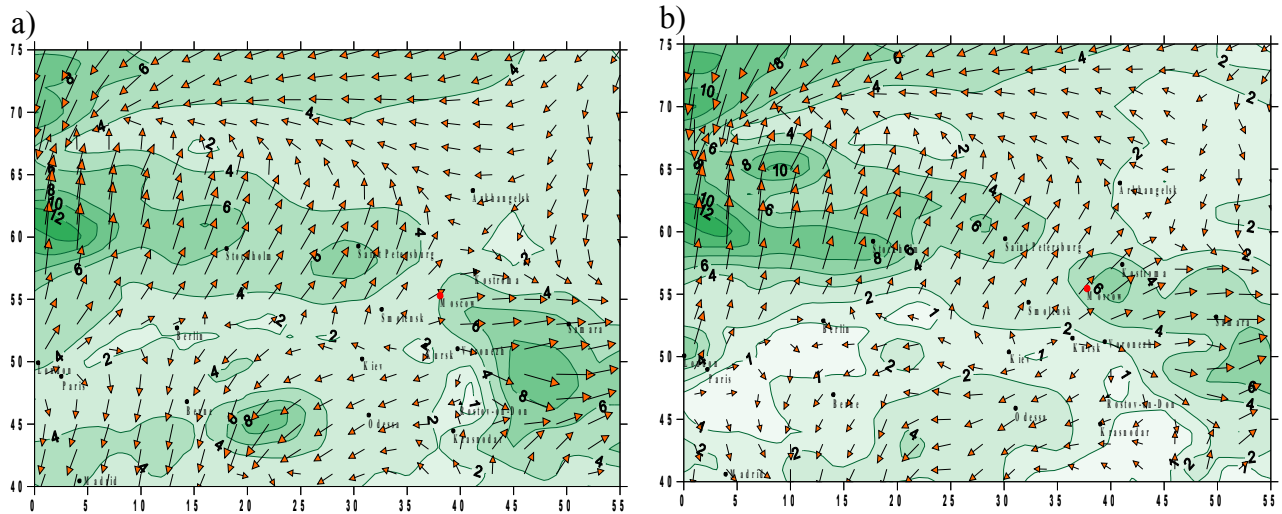
The wind direction error was 4 deg and the coefficient of correlation was equal 0.84 for entire calculation area when the prediction time period was 24 hour. The best accuracy of module wind was got in the areas where the wind velocity was more than 4m/s. But for the entire calculation domain the prediction accuracy was high too: the error was 0.32m/s and the correlation coefficient was 0.88 when the prediction time period was 24 hour.

So small errors for the surface wind prediction are an achievement of atmospheric boundary layer modeling in the numerical prediction operations conducted for the operational meteorological service.

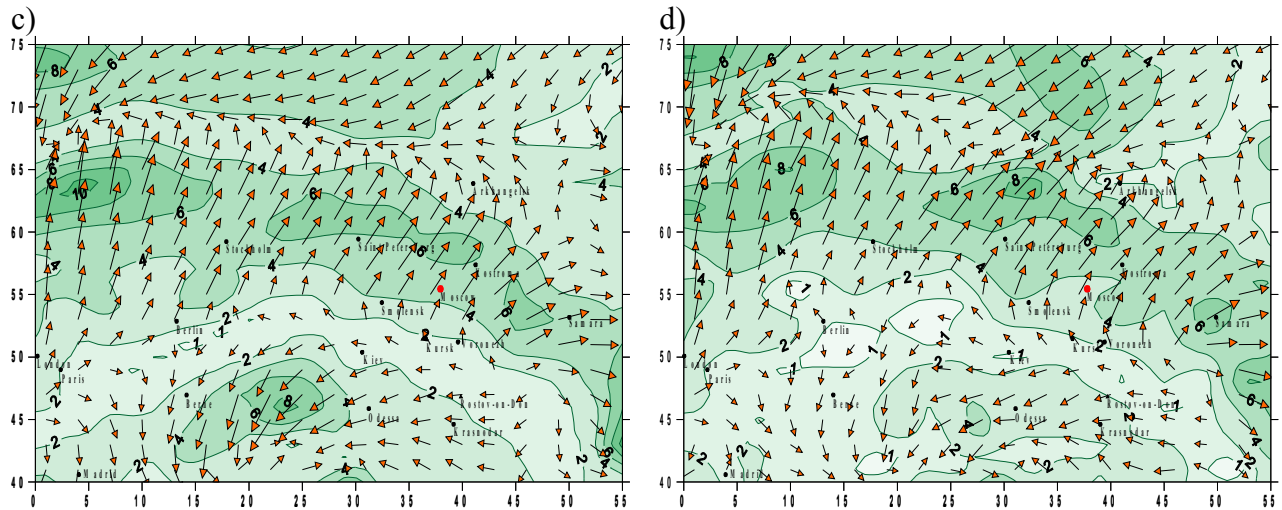
| Time period of prediction | Absolute error | Relative error | Correlation coefficient |
|---------------------------|----------------|----------------|-------------------------|
|---------------------------|----------------|----------------|-------------------------|

| Module of surface wind | | | |
|---------------------------|----------|------|------|
| 12 h | 0,77 m/s | 0,86 | 0,69 |
| 24 h | 0,32 m/s | 0,48 | 0,88 |
| 36 h | 0,97m/s | 0,57 | 0,89 |
| Direction of surface wind | | | |
| 12 h | 3 deg | 0,16 | 0,64 |
| 24 h | 4 deg | 0,16 | 0,84 |
| 36 h | 11deg | 0,26 | 0,69 |

12-hour prediction (a) and objective analysis (b) data of surface wind



24-hour prediction (c) and objective analysis (d) data of surface wind



References

Shnaydman, V., Berkovitch, L., 2006: Atmospheric Boundary Layer Modeling in the Numerical Prediction Operations, Research Activity in Atmospheric and Oceanic Modeling, No 36, 5.57-5.58

Progress and plans of the Météo-France NWP system in 2006: ARPEGE, ALADIN and AROME systems

François Bouttier and collaborators

(CNRM, Météo-France, 42 av. Coriolis F-31057 Toulouse France) e-mail: francois.bouttier@meteo.fr

1. NWP system overview

The operational NWP system of Météo-France mainly comprises two nested models, with their data assimilation system: the global ARPEGE, with a stretched T358c2.4L46 resolution (23km grid on Western Europe) with 6-hourly 4D-Var data assimilation, and the ALADIN-France LAM with a 3000x3000km domain around France at 9.5kmL46 resolution with 6-hourly 3D-Var data assimilation. Extra ARPEGE and ALADIN instances run with other geometries and data cutoffs for various operational purposes. A third nested model, AROME, is under development and aims for operational implementation in 2008 (1200x1200km 2.5kmL46 grid over mainland France).

In 2006 a major supercomputer upgrade took place. The Fujitsu vpp5000 platform was complemented by a 256-processor NEC SX8R machine, which is made of vector processors arranged in shared-memory clusters. Parallelisation can be achieved using OpenMP (inside each 8-processor cluster) or MPI. The upgrade amounts to a total x5 CPU upgrade with respect to the vpp5000 (i.e. 9Tflops peak performance), with an effective sustained speedup of approximately x3 (using the same number of processors) on the main NWP runs. The NEC SX8R will primarily be used to upgrade the ARPEGE and ALADIN resolutions (model and 4D-Var horizontal and vertical resolutions), and to allow a first real-time implementation of the AROME mesoscale model and its data assimilation.

More details are in <http://www.cnrm.meteo.fr/gmap/>

2. ARPEGE and ALADIN models

ARPEGE and ALADIN-France use the same physical parametrisations and model setup, except for the horizontal geometry and resolution. The main model physics upgrades in 2006 have been: an improved orography database and soil wetness climatology (from GSWP), with revised sea albedo and soil emissivity; introduction of a new prognostic cloud/precipitation microphysics scheme (adapted from Lopez 2002, with cloud water, cloud ice, rain and snow); revisions to the turbulence, shallow and subgrid convection (entrainment & cloudiness diagnostic) schemes; change of radiation scheme to use RRTM-IR adapted from ECMWF (16 IR and 2 visible bands).

Also, the vertical resolution has been improved from 41 to 46 levels, with the new levels in the upper stratosphere and above (the model top was raised from 1hPa to 5Pa). Some aspects of the semi-Lagrangian advection have been improved in the main model and in the linearized model used by 4D-Var.

These changes have improved the ARPEGE large-scale scores, e.g. the cloud products, with positive evaluation of ALADIN-France changes by the forecasters.

A very short cutoff 4D-Var analysis and forecast suite has been introduced shortly after 00UTC, on top of the regular 00UTC run (used for international WMO scores intercomparison) whose data cutoff was left unchanged. An extra ALADIN 3D-Var assimilation and forecast suite ran over Western Africa during the AMMA field experiment (June to September 2006).

The plans for 2007 focus on a major ARPEGE resolution upgrade, from T358L46 to T538L60 (with the same horizontal grid stretching factor $c=2.5$), which brings the resolution over Western Europe from 23km to 15km, and halves the vertical resolution in the upper troposphere and lower stratosphere. In the ARPEGE and ALADIN-France physics, it is planned to revise the subgrid orographic drag scheme, to further upgrade the radiation scheme, to make the Lopez microphysics scheme cheaper using a better sedimentation algorithm, to implement the SLHD adaptive horizontal diffusion scheme developed by the ALADIN consortium, to revise the representation of cirrus clouds and various physical aspects of the microphysics scheme. The AROME surface scheme (SURFEX) will be integrated into the ALADIN code in support of the ALADIN consortium's activities.

3. ARPEGE/ALADIN data assimilation

ARPEGE and ALADIN-France use about the same setup, except that ARPEGE uses an incremental 4D-Var analysis algorithm (with coupled OI surface analysis) whereas ALADIN uses nonincremental 3D-Var. Unlike ARPEGE, ALADIN 3D-Var assimilates Meteosat radiances. The major data assimilation upgrades in 2006 have been: assimilation of Quikscat scatterometer winds, of Aqua AMSU radiances, of MTSAT-1R atmospheric motion winds, of MODIS (Aqua and Terra) AMW winds near the poles, of extra AMSU channels, of SSM/I DMSP-F13 clear radiances, of AIRS (Aqua) radiances, of **ground-based GPS zenithal total delays** from European networks, plus upgrades to the radiosonde temperature and Meteosat radiance bias correction schemes, and upgrades to the SATOB and profiler data selection policy.

In the 4D-Var algorithm, the linearized stratiform precipitation scheme has been removed (it degrades the forecasts since the introduction of the Lopez physics in the main model); the variational observation quality control of ECMWF has been activated. Flow-dependent quality control thresholds are now used, thanks to a (six-member) randomization technique that estimates background standard errors in the 4D-Var cost function. The 4D-Var minimization now uses 25

iterations in each of the two inner loop minimizations (it was 40+15 previously).

The plans for 2007 include an upgrade to the 4D-Var increment resolution from T149L46 to T224L60, the introduction of a non-linear balance and a new humidity variable in 4D-Var and 3D-Var, the use of GPS COSMIC radio-occultation data, of several instruments onboard the Metop satellite, and SSMI/S radiances.

4. The AROME system

The AROME model has been running daily throughout 2006 without any major problem. Also, it has been tested on various domains, including equatorial Africa (the AMMA field experiment), central Turkey, and several central European and nordic domains (runs by the ALADIN and HIRLAM consortia). All these runs - in research mode and in dynamical adaptation of lower resolution models - gave a broad view of the AROME performance. The model appears to be very robust and gives reasonable results in all weather situations. The model technical setup is still cumbersome and it is being simplified. The most obvious strength of the model is the ability to give strong precipitation warnings in situation of strong deep convection. The most obvious weaknesses have been the low-level parameter biases and the cloud cover forecasts.

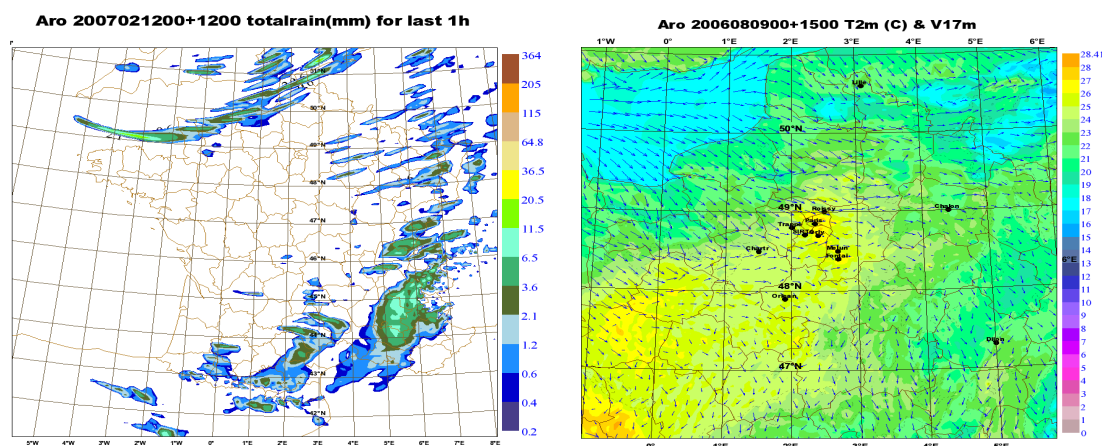
Low-level forecast errors, as diagnosed using scores against SYNOP data, have been traced back to bugs in the physiography setup, and to weaknesses in the vertical interpolation formulae used in the PBL below the model's lowest mass level. Improved formulae (e.g. using the Paulsen approach) have alleviated some night-time biases, which improves the AROME T2m/RH2m objective scores to the extent that they now consistently beat the ALADIN-France scores. A lack in low level cloudiness has been attributed to deficiencies in the representation of shallow convection at the top of the PBL. Thus, a subgrid shallow convection scheme has been introduced in AROME, using a combination of the Kain-Fritsch-Bechtold scheme (shallow part) and

a new closure based on an eddy-damped mass-flux approach (P. Soares). This improved the forecast PBL vertical thermodynamical profiles and created more realistic cumulus cloud structures. Work in this area is still ongoing. A third deficiency of AROME is the handling of narrow valleys. The semi-lagrangian formulation of the AROME non-hydrostatic dynamics is rather smoothing, which means that very local features (e.g. pockets of cold air below inversions) are not well represented in valleys where the width is less than twice the model numerical grid size. Experiments have been carried out with various horizontal diffusion schemes (so-called SLHD semi-Lagrangian scheme) to try and minimize this behavior.

Other advances in AROME physics include a better representation of fog (including aerosol dependency and sedimentation of fog droplets), the introduction of a prognostic snow scheme, tests of interactive ocean mixed layer schemes, improvements to the cloud/radiation interaction, and the development of an experimental version of AROME with interactive chemistry, dust and aerosols. The physics/dynamics interface is being revised in order to improve code interoperability with other developments of the ALADIN consortium.

The AROME data assimilation is being adapted from the ALADIN 3DVar system to a higher resolution ($dx=2.5km$). A variational background error term (the so called J_b) was computed using AROME ensemble forecasts, forced by ARPEGE ensemble data assimilations. The corresponding structure functions are quite sharp, and sensitive to the vertical stratification: anticyclonic and convective weather produces very different forecast error covariances. Finally, radar processing has been implemented in AROME 3DVar, and first assimilation experiments of Doppler wind components are promising.

The AROME daily runs have been upgraded to cover the whole mainland France and Corsica using daily 30-h forecasts, in January 2007.



Two samples of AROME real-time forecast fields: a winter frontal rain event over France (left panel; the colors represent 1-hourly liquid rainfall), and a summertime afternoon with a heat island effect on Paris (right panel; the colors represent 2m temperature, the arrows represent 10m wind).

Resolution dependence of hydrometeor structures generated by cloud resolving model

Hisaki Eito and Kazumasa Aonashi

Meteorological Research Institute, Japan Meteorological Agency

1-1, Nagamine, Tsukuba, Ibaraki, 305-0052, Japan

E-Mail: heito@mri-jma.go.jp

1. Introduction

Cloud Resolving Models (CRMs) with complicated cloud physical parameterization forecast various cloud physical variables with high resolution in time and space. Microwave radiometer brightness temperatures (MWR TBs) are sensitive to water vapor, cloud liquid water, and precipitation, assimilation of MWR TBs to CRMs will be of great use. However, cloud physical validation of CRMs has not sufficiently been carried out.

This paper investigates the characteristics of forecasting of hydrometeors and sensitivities with the bulk cloud microphysics scheme of the CRM for observed snow clouds over the Sea of Japan. Special attention will be given to sensitivities of CRM's horizontal resolution to the hydrometeors forecasting.

2. Cloud resolving model

The CRM developed by Japan Meteorological Agency (JMA) is used in this study (JMANHM: Saito *et al.*, 2006.). The bulk cloud microphysics scheme is employed in the JMANHM. This scheme predicts the mixing ratios of six water species (water vapor, cloud water, rain, cloud ice, snow and graupel) and number concentrations of ice particles (cloud ice, snow and graupel).

3. Results

The JMANHM successfully reproduced the observed features of snow clouds. However, in comparison spaceborne microwave radiometer observations and airborne in situ observations with the model simulations, the model overpredicted the mass concentrations of snow, but underpredicted the amount of cloud liquid water and graupel. In the model, depositional growth of snow was dominant due to the increase in the number concentration of snow by conversion of cloud ice to snow. Snowfall speeds, ice nucleation processes and vertical wind velocities related to the horizontal grid size of the model were sensitive to reduction of snow overprediction..

A set of experiments were conducted using different horizontal resolutions to quantify the resolution sensitivities. Initial and boundary conditions for a separate 1-km run, 0.5-km run, 0.25-km run and 0.125-km run are obtained by

using hourly forecast from 2-km run. Figure 1 shows time series of area-averaged (135-136E, 37-38N) 1-h precipitation. There is no remarkable difference in each simulation on surface precipitation forecast. Horizontal distributions of vertically integrated total condensed water simulated by the 1- and 0.125-km simulations are shown in Fig. 2. Distribution of total water of 0.125-km simulation is almost similar to that of 1-km simulation except for dominance of smaller scale structures. Vertical profiles of horizontally averaged total condensed water amount and each hydrometeors amount are shown in Fig. 3. There is also no remarkable difference in each simulation on total condensed water forecast. Those simulations with higher resolution have larger amount of graupel and cloud water and smaller amount of snow relative to those with lower resolution; however, the result of 0.5-km run is almost closed to convergence.

Figure 4 shows vertical profiles of horizontally averaged vertical velocities. In the area-averaged vertical velocity field (Fig. 4a), those simulations with higher resolution have larger value of the maximum of averaged vertical velocities relative to those with lower resolution. The result of 0.5-km run is also closed to convergence, which is consistent with result in hydrometeor structures. In contrast, the amplitude of vertical velocity increases with mesh size becoming small (Fig. 4b). Furthermore, the height of peak value lowers. The increasing of amplitude of vertical velocity is remarkable under the bottom of clouds, indicating that it has a small effect on hydrometeor's production. These results suggest that simulation with $dx \sim 0.5$ -km resolution is enough to produce structures of vertical velocity related to hydrometeors of snow clouds in this case.

Additional cases (e.g. other snow clouds and/or summer deeper convective clouds) will be analyzed to verify microphysical sensitivities of CRM presented in this case.

Acknowledgments

This research was mainly supported by the fund of Japan Science and Technology Agency - Core Research for Evolutional Science and Technology.

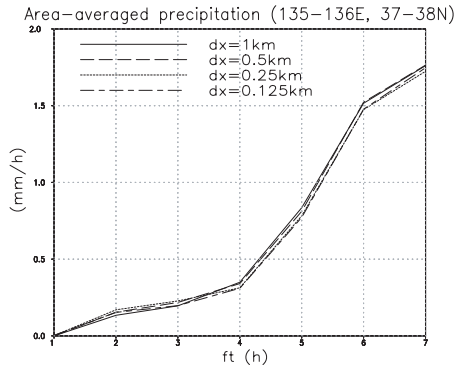


Fig. 1. Time series of area-averaged (135-136E, 37-38N) 1-h precipitation derived from 1- (solid), 0.5- (broken), 0.25- (dotted) and 0.125-km (dashed) experiments until 5 hours forecast.

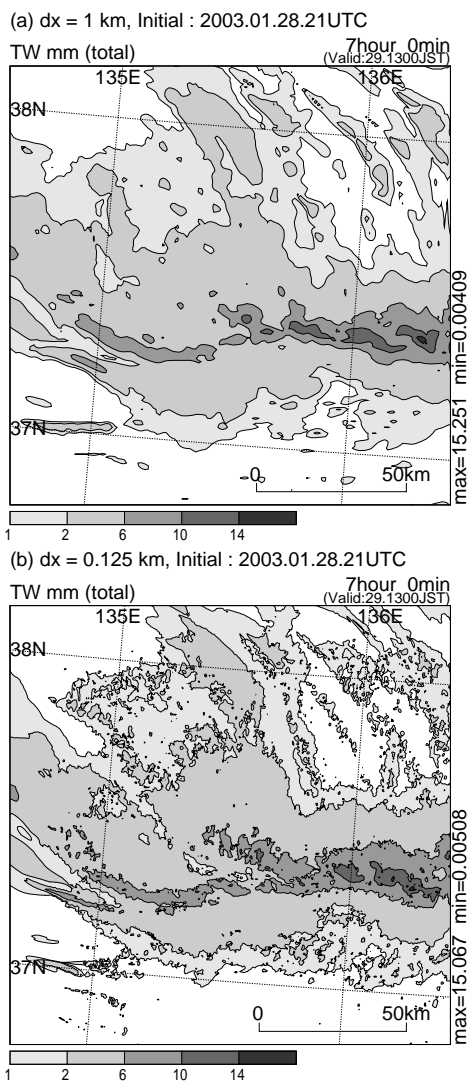


Fig. 2. Vertically integrated total condensed water for the (a) 1- and (b) 0.125-km experiments at 1300 LST 29 Jan. 2003 (5 hours forecast).

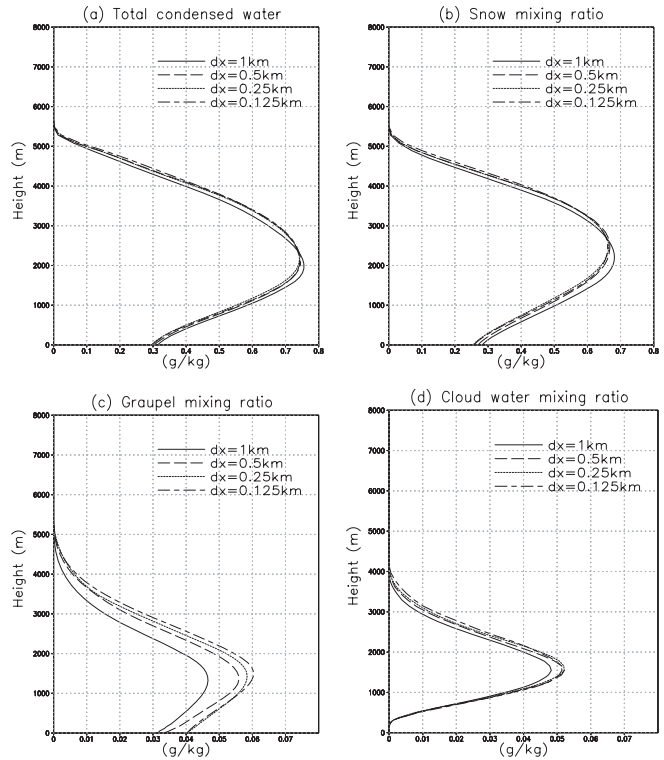


Fig. 3. Vertical profiles of horizontally-averaged (135-136E and 37-38N) (a) total condensed water, (b) snow mixing ratio, (c) graupel mixing ratio and (d) cloud water mixing ratio derived from 1- (solid), 0.5- (broken), 0.25- (dotted) and 0.125-km (dashed) experiments at 1300 LST 29 Jan. 2003 (5 hours forecast).

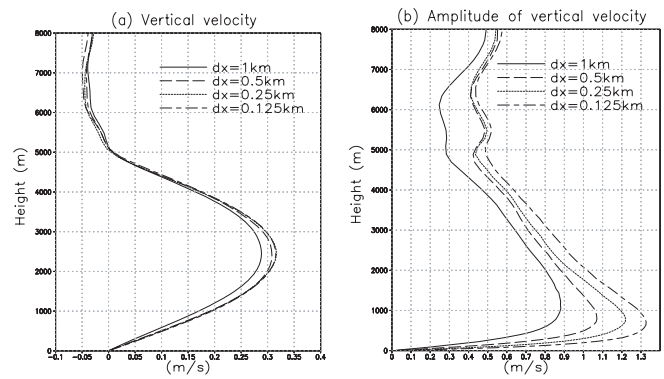


Fig. 4. Vertical profiles of horizontally-averaged (135-136E and 37-38N) (a) vertical velocities and (b) amplitude of vertical velocities derived from 1- (solid), 0.5- (broken), 0.25- (dotted) and 0.125-km (dashed) experiments at 1300 LST 29 Jan. 2003 (5 hours forecast).

Reference

Saito, K., T. Fujita, Y. Yamada, J. Ishida, Y. Kumagai, K. Aranami, S. Ohmori, R. Nagasawa, S. Tanaka, C. Muroi, T. Kato and H. Eito, 2006a: The operational JMA nonhydrostatic mesoscale model. *Mon. Wea. Rev.*, **134**, 1266-1298.

1. CONTEXT

Météo-France regional center based in La Réunion island provides different kinds of meteorological assistances : general weather forecasts focused on La Réunion island, marine weather forecasts over the whole southwest Indian ocean and, as a RSMC¹, tropical cyclone watching, an international duty entrusted by the WMO².

To achieve these tasks, Météo-France forecast teams have at their disposal a new weather prediction model since October 2006, called Aladin-Réunion³ and covering their area of interest (figure 1).

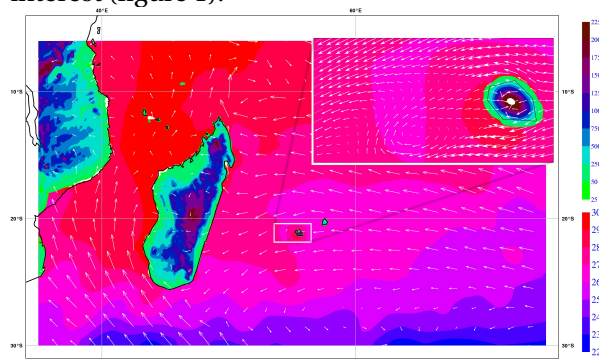


Figure 1 : ALADIN-Réunion domain on which have been plotted its relief (in m) and its sea surface temperature (°C) and 10m wind (arrows) analysis on the 12 december 2006 at 12UTC. A zoom over La Réunion, in the upper right panel, shows the complex effect of the island orography on the wind.

2. MODEL DESCRIPTION

The limited area model run over the south west Indian ocean is the Aladin model (Bubnová et al, 1993 ; Radnóti et al, 1995 ; Horányi et al, 1996) coupled with Météo-France global model Arpege⁴ (Courtier et al, 1991) at a uniform resolution. The domain roughly covers the RSMC zone of La Réunion. It has its own assimilation scheme which uses the 3D Var algorithm (Courtier et al, 1998) with a six hour window and a linear beta-plane balance. In the following, the observations dataset is the same

1 RSMC : Regional Specialized Meteorological Center
2 WMO : World Meteorological Organization
3 ALADIN-Réunion : Aire Limitée Adaptation Dynamique Internationale-Réunion
4 ARPEGE : Action de Recherche Petite Echelle Grande Echelle

as the one from the coupling model which contains in particular a mean sea level pressure bogus. The forecast model is run at the same resolution (10 km) as the analysis. The calculation grid is linear. The background errors covariances have been computed with the analysis ensemble technique (Berre et al, 2006) on warm season meteorological conditions.

3. LIMITED AREA MODEL PERFORMANCES

Aladin-Réunion with its 10km horizontal resolution stands as a significant improvement compared to the global models available over this region, the resolution of which is comprised between 55 and 25km. The better representation of the steep relief of La Réunion, a 2500km² island which reaches its highest point above 3000m, enables the model to forecast more realistic interactions between the orography and the atmosphere (figures 1 and 2).

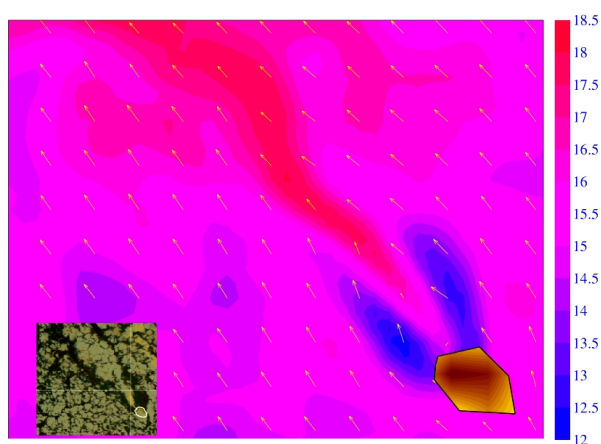


Figure 2 : ALADIN-Réunion forecasts based on the 28 June 2006 at 00UTC valid for the following day at 00UTC. The wet pseudo-adiabatic temperature Θ'_w at 925hPa (colored area in °C) and 10m wind (arrows) are plotted. For comparison, the NOAA18 colour composite on the 28 June 2006 at 23UTC is shown in the bottom left panel. ALADIN-Réunion can remarkably forecast the cloud plume leeward of the island.

This limited area model can also simulate cyclones with a better structure than the global models ones ; on figure 3, the maximum wind radius analysed by Aladin is in better agreement with the reality than Arpege's one. This more realistic analysis has a positive impact on all

ranges of the two day forecast track (figure 4).

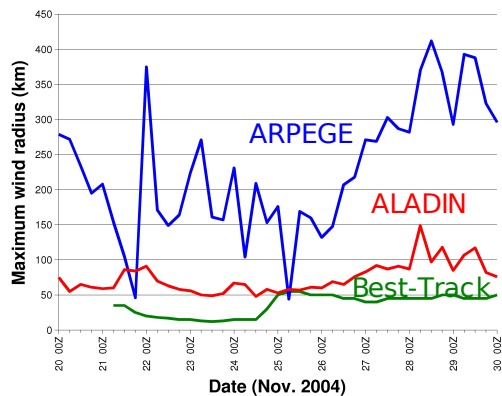


Figure 3 : Radius of maximum wind analysed by the forecasters, Arpege and Aladin on cyclone Bento (November 2004)

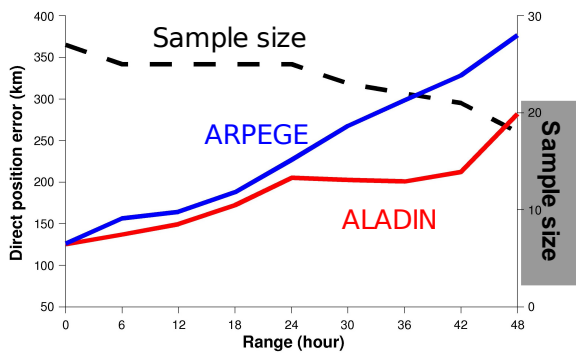


Figure 4 : Evolution of direct position error with range averaged over four cyclone cases : Bento, (november 2004), Juliet (April 2005), Daren and Ernest (January 2006).

4. PERSPECTIVES

Ongoing tests on a three-dimensional wind vortex significantly improve the analyzed position of cyclones, and by consequence their forecast position. Non linear and omega balances (Fisher, 2003), that make the background covariance model dependent on the flow, i.e. forcing the background errors to be spatially heterogeneous, have been experimented and lead to a very positive signal for cyclone analyses. These new releases should be operational for the next cyclonic season. Efforts are also gathered on the humidity field initialization by assimilating SSM/I⁵ radiances in cloudy and rainy conditions. In regard to intensity forecasts, the impact of a high resolution sea surface temperature analysis is being tested.

5 SSM/I : Special Sensor Microwave Imager

5. REFERENCES

- Berre, L., S.E., Stefanescu, and M. Belo Pereira, 2006: The representation of the analysis effect in three error simulation techniques. *Tellus*, 58, 196-209.
- Bubnová, R., A. Horányi and S. Malardel, 1993: International Project ARPEGE/ALADIN. *EWGLAM Newsletter*, 1993, 117-130.
- Courtier, Ph., C. Freydl, J.F. Geleyn, F. Rabier and M. Rochas, 1991: The ARPEGE project at METEO FRANCE. *ECMWF Seminar Proceedings* 9-13 September 1991, Volume II, 193-231.
- Courtier, P., E. Andersson, W. Heckley, J. Pailleux, D. Vasiljevic, M. Hamrud, A. Hollingsworth, F. Rabier and M. Fisher, 1998: The ECMWF implementation of three-dimensional variational assimilation (3D-Var). Part 1: formulation. *Quart. J. Roy. Meteor. Soc.*, 124, 1783-1807.
- Fisher, M., 2003: Background error covariance modelling. In Recent developments in data assimilation for atmosphere and ocean, *ECMWF Seminar proceedings*, 45-63.
- Horányi, A., I. Ihász, and G. Radnóti, 1996: ARPEGE/ALADIN: A numerical weather prediction model for Central-Europe with the participation of the Hungarian Meteorological Service. *Időjárás*, 100, pp 277-300.
- Radnóti G., R. Ajjaji, R. Bubnová, M. Caian, E. Cordoneanu, K. Von Der Emde, J.D. Gril, J. Hoffman, A. Horányi, S. Issara, V. Ivanovici, M. Janousek, A. Joly, P. Le Moigne, S. Malardel (1995): The spectral limited area model ARPEGE/ALADIN. *PWPR Report Series n°7*, WMO-TD n° 699, pp. 111-117.

Upgrade of the operational JMA non-hydrostatic mesoscale model

TABITO HARA¹, KOHEI ARANAMI, RYOJI NAGASAWA, MASAMI NARITA, TOMONORI SEGAWA,
DAISUKE MIURA, YUKI HONDA, HIROSHI NAKAYAMA AND KENSUKE TAKENOUCHE

*Numerical Prediction Division, Japan Meteorological Agency,
1-3-4, Otemachi, Chiyoda-ku, Tokyo 100-8122, Japan*

1 Introduction

The Japan Meteorological Agency (JMA) has been operating the mesoscale model(MSM) since March 2001 to provide short time scale forecasts for preventing disaster. MSM covers the domain near Japan which expands 3600 km from east to west, and 2900km from north to south.

While the first MSM was a hydrostatic model with 10-km horizontal resolution and 18-hour forecast 4 times a day, it was replaced by a non-hydrostatic model (JMANHM) on Sep.1, 2004[1] with the same domain, horizontal resolution, forecast time and frequency as the hydrostatic one. The differences between the former hydrostatic model and JMANHM were not only in dynamics frame, but also in many physical processes such as cloud microphysics and Kain-Fritsch cumulus convective parameterization scheme.

In March 2006, its horizontal and vertical resolution and forecast frequency was enhanced corresponding to the renewal of supercomputer system : horizontal resolution was increased to 5-km, the number of vertical layers were raised from 40 to 50, and 15-hour forecasts are operated every 3 hours, or 8 times a day[2]. Physical processes were also improved so that it could give more accurate forecasts, especially for precipitation and surface temperature and wind.

We also plan to extend forecast time from 15 to 33 hours 4 times a day out of 8 time forecasts in May 2007. In this report, the specifications of JMANHM of the next version which is planned to replace the current operational MSM in May 2007 is mentioned. The current operational MSM and the improved MSM are denominated MSM0603 and MSM0705 respectively below.

2 Specifications of MSM0705

The specifications of MSM0705 compared with MSM0603 are shown. Although the trigger of this replace of MSM model is to expand forecast time from 15 hours to 33 hours, many processes (mainly physical processes) are improved from the current one.

Basic frame The forecast domain, horizontal resolution, and number of grids of MSM0705 are the same as MSM0603.

Dynamics The generalized hybrid vertical coordinate is introduced instead of z^* coordinate[3]. While the model planes at lower layers are following terrain, those at higher layers are made horizontal to reduce errors of calculating pressure gradient force and advection.

Turbulence process Improved Mellor-Yamada Level 3 scheme[4] is implemented[5], in which parameters on the closure assumption are revised from orig-

inal Mellor-Yamada model by referring to the latest LES results, and time integration of variables on turbulence(ex. TKE) is made more stable. This scheme provides more accurate expression of boundary layer. As the surface flux scheme, the scheme by Beljaars and Holtslag[6] is adopted instead of Louis[7] on land and Kondo[8] on sea.

Radiation process The clear sky radiation scheme is replaced by that of the latest operational global model of JMA(GSM), which reduces biases of heating rate by long wave radiation. Cloud fraction and cloud water which are needed by radiation scheme to evaluate the effect of clouds are calculated by partial condensation scheme instead of by the diagnosis from relative humidity and total precipitation water. The normal distribution on vapor amount is assumed and its standard deviation is evaluated by the outputs from turbulent schemes. It makes representation of cloud more realistic. Consequently reduction of bias of shortwave radiation flux toward surface is confirmed, and more diurnal change of surface temperature is favored.

Moisture process Finite terminal velocity is given to cloud ice in cloud physics, which had been assumed not to fall. It removes excessive cloud ice which is accumulated with the progress of forecast time and make a harmful effect on radiation process. As to cumulus convective parameterization, the relative humidity based perturbation is added to the trigger function of Kain-Fritsch scheme to remove excessive precipitation by grid scale convection and precipitation is made less sensitive to terrain and surface roughness.

3 Verification of MSM0705

To display the performance of MSM0705, the statistical verifications of MSM0705 for precipitation, surface temperature, and vertical profile of temperature compared with MSM0603 (of which forecast period is simply expanded to 33 hours with MSM0603 to compare the performance of models) in July 2006 (summer term) and January 2006 (winter term) are shown.

In verifying precipitation, threat score and bias score are evaluated comparing with radar observations calibrated by rain gauge observations with 20-km verification grid. Fig.1 shows the time series of threat score and bias score for precipitation of 10-mm per 3 hours in summer and 5-mm per 3 hours in winter with forecast time. The threat score of MSM0705 is better than MSM0603 through almost forecast time in both summer and winter.

Mean error (or bias) and root mean square error (RMSE) of surface temperature for each valid time compared with AMeDAS (Automated Meteorological Data Acquisition System of JMA: about 900 points which provide temperature and wind observations

¹E-mail: tabito.hara@met.kishou.go.jp

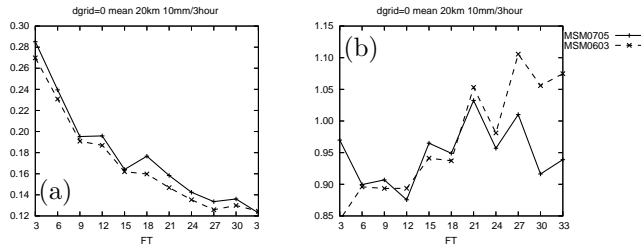


Fig. 1: Verification of precipitation. (a) Time sequence of threat score for 10 mm per 3 hours in summer. (b) Same as (a) but of bias score. Solid line, dashed line indicate MSM0705 and MSM0603 respectively.

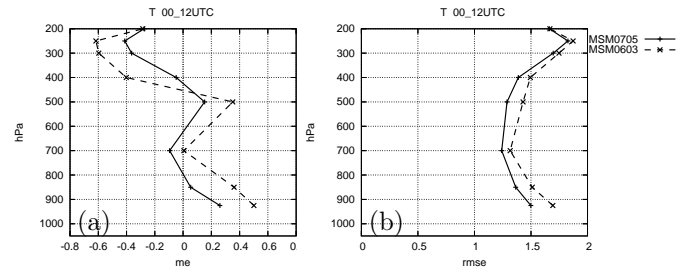


Fig. 3: Verification of vertical profile of temperature at forecast time 33 hours. (a) Vertical profile of ME in summer. (b) Same as (a) but of RMSE.

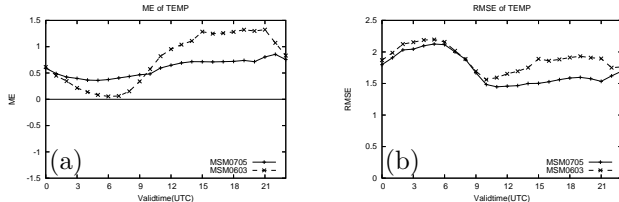


Fig. 2: Verification of surface temperature for each valid time. (a) Time sequence of ME in summer. (b) Same as (a), but of RMSE.

across Japan) are displayed in Fig.2. The diurnal changes of bias become smaller, or the more realistic diurnal changes of surface temperature and wind are exhibited. (In this summer term, bias in the daytime is positive and the positive bias becomes increased, but this case is unusual and bias in the daytime usually is negative. The smaller diurnal change of bias should be attracted.)

Bias and RMSE of vertical profile of temperature at forecast time 33 hours compared with sonde observations are shown in Fig.3. Decrease of bias and RMSE is found, especially in summer term.

In this way, it is confirmed that MSM0705 is superior to MSM0603.

4 Example of forecast by MSM0705

Example of forecast by MSM0705 is shown in Fig.4. Although the position of rainband differs a bit from the observation, MSM0705 gives much better expression for the rainband than the current MSM.

5 Conclusion and remarks

MSM is improved by many development, especially in physical processes, and will be operational in May

2007. Further developments to advance dynamical and physical processes more and to operate in higher resolution are going on.

References

- [1] K.Saito, T.Fujita, Y.Yamada, J.Ishida, Y.Kumagai, K.Aranami, S.Ohmori, R.Nagasawa, S.Kumagai, C.Muroi, T.Kato, H.Eito, and Y.Yamazaki. The Operational JMA Nonhydrostatic Mesoscale Model. *Mon. Wea. Rev.*, 134, 1266–1298, 2006.
- [2] K.Aranami and T.Segawa. Verification of mesoscale forecasts by a high resolution non-hydrostatic model at jma. *CAS/JSC WGNE Res. Activ. Atmos. Oceanic Modell.*, 36, 66–67, 2006.
- [3] J.Ishida. Development of a hybrid terrain-following vertical coordinate for jma non-hydrostatic model. *CAS/JSC WGNE Res. Activ. Atmos. Oceanic Modell.*, 37, 2007.
- [4] M. Nakanishi and H. Niino. An improved mellor-yamada level-3 model: Its numerical stability and application to a regional prediction of advection fog. *Bound.-Layer Meteor.*, 119, 397–407, 2006.
- [5] T.Hara. Implementation of improved mellor-yamada level 3 scheme and partial condensation scheme to jmanhm and their performance. *CAS/JSC WGNE Res. Activ. Atmos. Oceanic Modell.*, 37, 2007.
- [6] A. C. M. Beljaars and A. A. M. Holtstag. Flux parameterization over land surfaces for atmospheric models. *J. Appl. Meteor.*, 30, 327–341, 1991.
- [7] J.F. Louis, M.Tiedtke, and J.F. Geleyn. A short history of the operational pbl parameterization at ECMWF. In *Proc. Workshop on Planetary Boundary Layer Parameterization*, pages 59–79, Reading, United Kingdom, 1982. ECMWF.
- [8] J. Kondo. Air-sea bulk transfer coefficients in diabatic conditions. *Bound. Layer Met.*, 9, 91–112, 1975.

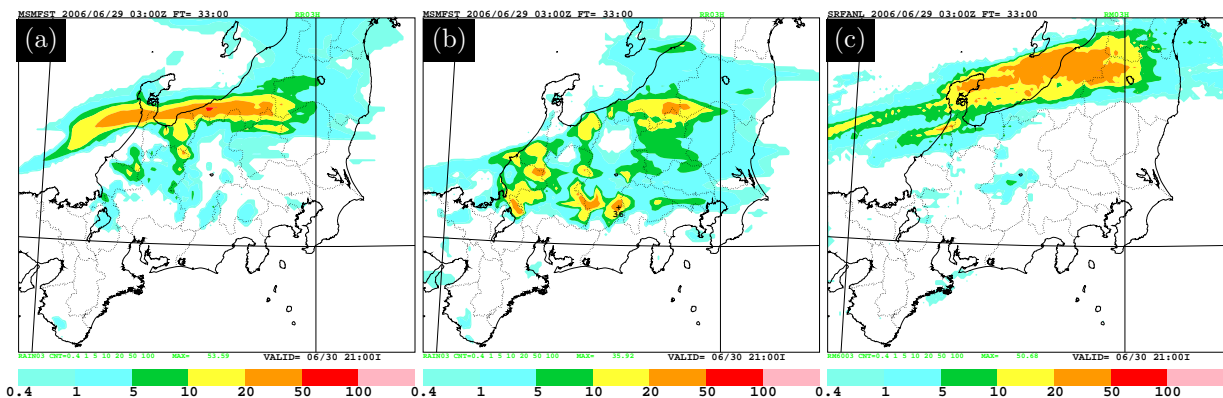


Fig. 4: (a) Forecasted 3-hour accumulated precipitation at forecast time 33 hours by MSM0705. Initial time is 0300 UTC 29 Jun 2006. (b) Same as (a), but by MSM0603. (c) observation at the time corresponding to the forecasts.

Relation of Dec. 2005 heavy snowfall and cloud-top heights around the Japan-Sea side of the Japan Islands, estimated from objective analyses and forecasts of cloud-resolving model

Teruyuki KATO* and Syugo HAYASHI*

*Meteorological Research Institute / Japan Meteorological Agency, 1-1 Nagamine, Tsukuba, Ibaraki 305-0052, Japan

Cloud-top heights of cumulonimbi are almost estimated from the level of neutral buoyancy (LNB). A low-level humid air is lifted adiabatically from the originating level to the lifting condensation level along the dry adiabat, and it is lifted further along the moist adiabat. The upper point at which the moist adiabat crosses the profile of temperature is the LNB. The higher equivalent potential temperature makes the LNB higher. Over the Sea of Japan in winter, a near-surface air gets sensible and latent heat from relatively warm sea surface. This air-mass transformation becomes larger when the fetch becomes longer and the temperature distance between sea surface and cold air-mass becomes larger. Therefore, the low-level equivalent potential temperature becomes higher around the Japan-Sea side of the Japan Islands, and consequently cloud-top heights become higher there. It should be noted that the Japan Islands are located on the downstream side of the Sea of Japan for the winter monsoon (i.e., northwesterly winds).

The LNB around the Japan-Sea side of the Japan Islands is statistically examined using 6-hourly Regional Objective Analysis Data (RANAL, horizontal resolution: 20 km) of the Japan Meteorological Agency (JMA). The statistical period is December and January in 2001-2005 winter seasons. The relation between Dec. 2005 heavy snowfall and cloud-top heights is comparatively examined from the horizontal distributions of averaged LNB in Dec. 2005 and the other years. The averaged LNB in 2005 is higher than 700 hPa, and it becomes exceeding 50 hPa higher than that in the other years. The appearance rate of LNB in 2005 is also 20-30 % higher. Therefore, heavy snowfall in Dec. 2005 was caused by the environmental condition under which cumulonimbi not only easily form, but also develop higher.

The consistency between cloud-top heights and the above-mentioned LNB is examined using the simulated results of a cloud-resolving model (JMA nonhydrostatic model (Saito et al 2006) with the horizontal resolution of 1 km, 1km-CRM). The initial and boundary conditions of 1km-CRM are produced from the 12-hour forecasts of JMA nonhydrostatic model with the horizontal resolution of 5 km (5km-NHM). The initial and boundary conditions of 5km-NHM are produced from the RANAL. The precipitation in 1km-CRM is calculated using a bulk-type microphysics scheme in which the mixing ratios of cloud and ice cloud, rain, snow and graupel are predicted. In 5km-NHM, the Kain-Fritsch convective parameterization scheme is used conjunctionally with a microphysics scheme. 9-hour forecasts are performed 4 times a day by the 1km-CRM, and 3-9 hour predicted data are used in

this statistical study. The rainfall distribution predicted by the 1km-CRM (Fig. 4a) well reproduced that of JMA Radar-Raingauge analyzed precipitation (R-A, not shown), although the rainfall amount is overestimated. This overestimation could be brought from the underestimation of R-A.

Figure 1a shows the horizontal distribution of averaged cloud-top heights in Dec. 2005 simulated by the 1km-CRM. Higher cloud-top heights are found over plain areas (about 680 hPa). Meanwhile, cloud-top heights are relatively lower over mountainous areas, because clouds formed by updrafts on the slope are included. The vertical profiles of appearance rate of predicted cloud-top heights (Fig. 2a) show that the LNB over a 600-hPa level in Dec. 2005 appears exceeding two times more frequently than in Jan. 2006, and the vertical level with the maximum frequency is exceeding 50 hPa higher. In other words, the higher development of snow clouds caused the heavy snowfall in Dec. 2005.

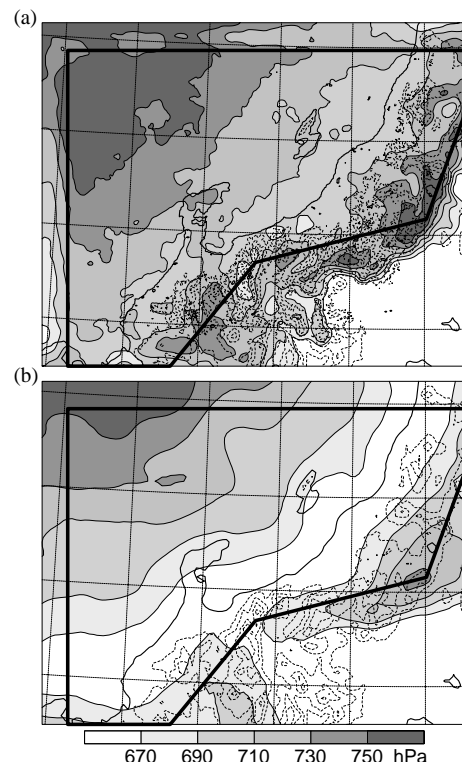


Fig. 1 Horizontal distribution of averaged cloud-top heights in Dec. 2005 predicted by (a) the 1km-CRM and (b) 5km-NHM. Cloud-top heights are determined by the threshold value of hydrometeor mixing ratio 0.1 g kg^{-1} . Broken lines denote the topography with intervals of 500 m.

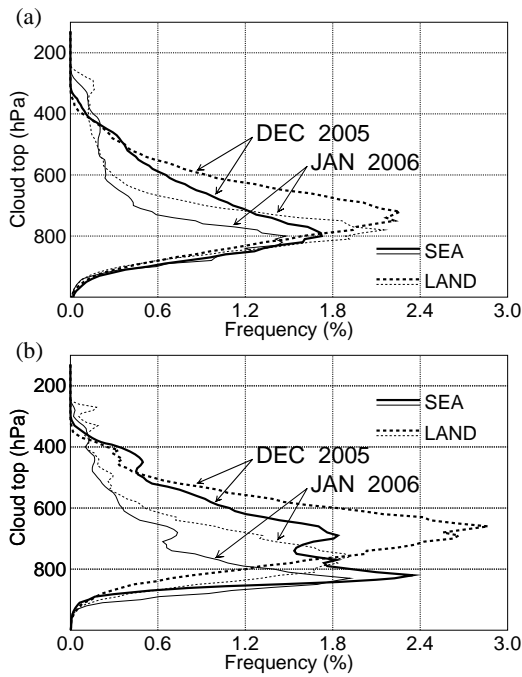


Fig. 2 Vertical profiles of appearance rate of cloud-top heights, found over grids points with updrafts, predicted by (a) 1km-CRM and (b) 5km-NHM. Each rate is calculated by dividing the heights into 100 vertical levels with an interval of 1 hPa

The vertical profiles of appearance rate of LNB (Fig. 3a), estimated from the results of CRM, well correspond with those from the RANAL. In the profile of Dec. 2005 over the sea, the appearance rate of LNB over a 600-hPa level is remarkably higher than that of Jan. 2006. The comparison of heights between cloud tops and LNB shows that cloud-top heights appear with about an half frequency of LNB, and the vertical profiles of appearance rates of LNB over the sea are very similar to those of cloud-top heights on the land. This indicates that snow clouds forming over the sea develop on the land.

For the averaged cloud-top heights in Dec. 2005, the results of 5km-NHM (Fig. 1b) are higher about 50 hPa than those of 1km-CRM (Fig. 1a). Meanwhile, such differences are never found for the averaged LNB (not shown). These indicate that cloud-top heights are differently simulated for the horizontal resolution and the treatment of moist convection. The above-mentioned features are ascertained from the relation of appearance rate distributions between cloud-top heights (Fig. 2) and LNB (Fig. 3). Rainfall amount over plain areas and near the coast is less simulated by the 5km-NHM than the 1km-CRM, and the rainfall of 5km-NHM is concentrated over mountainous regions. Meanwhile, the rainfall distribution of 1km-NHM is well similar to the R-A (not shown).

In comparison with the results of 1km-CRM, the 5km-NHM overestimates cloud-top heights (Fig. 2), and it underestimates rainfall amount over the plain and near the coast (Fig. 4) although the appearance

rate of cloud-top heights overestimates there (Fig. 3). This cause will be examined from the distribution of simulated hydrometeors and diabatic heating. Further, for our future works, the relation of predicted cloud-top heights by the 1km-CRM to those observed by meteorological radars should be examined.

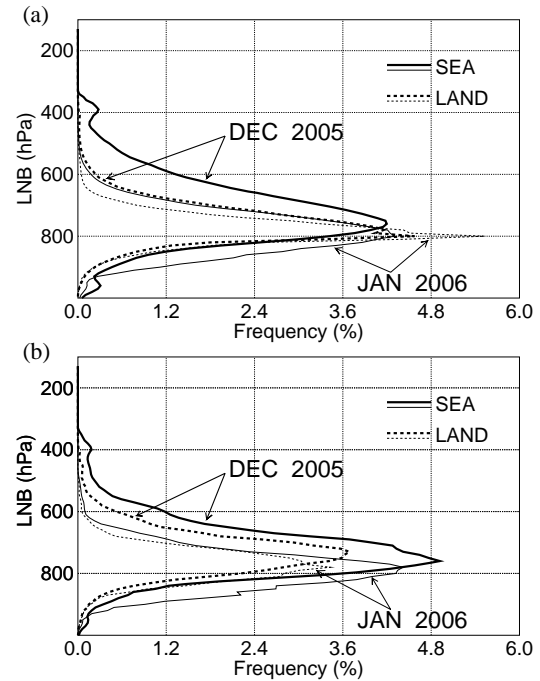


Fig. 3 Same as Fig. 2, but for the LNB that is estimated by lifting an air around a 20-km height.

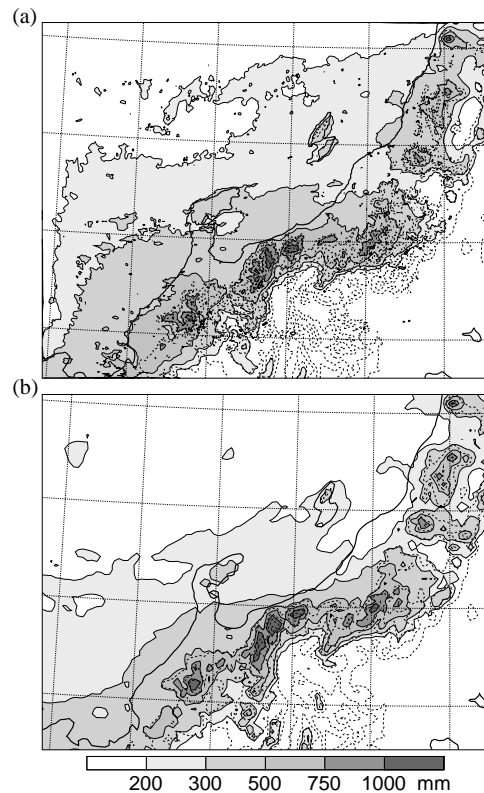


Fig. 4 Same as Fig. 1, but for the monthly accumulated rainfall.

Numerical simulation of tornado-producing supercell storm and tornado associated with Typhoon Shanshan (2006)

Wataru Mashiko

Meteorological Research Institute, JMA, 1-1 Nagamine, Tsukuba, Ibaraki 305-0052, Japan
(E-mail : wmashiko@mri-jma.go.jp)

1. Introduction

On 17 September 2006, three tornados hit the Miyazaki Prefecture, western Japan, during the passage of the rainband of Typhoon Shanshan. The tornado which hit Nobeoka city caused most severe damage and was assessed with F-2 scale. In order to reveal the environmental field and the storm which spawned the tornados, the numerical simulations were conducted. Moreover, the high-resolution simulation with the horizontal grid spacing of 50 m was attempted to reproduce the tornado explicitly.

2. Numerical model

The numerical model used in this study is the fully compressible nonhydrostatic model developed by Japan Meteorological Agency (JMANHM; Saito et al. 2006). We employed the bulk-type cloud microphysics scheme with six water species (water vapor, cloud water, rain, cloud ice, snow and graupel) and the turbulent closure scheme that predicts the turbulent kinetic energy. As to the surface boundary condition, exchange coefficients of surface fluxes are determined from the formula by Kondo (1975) over the sea and they are based on Monin and Obukhov's similarity law over the land, depending on the roughness and temperature. To conduct the high-resolution model integration, four telescoping one-way nested grids (Horizontal grid spacing 5 km; NHM5km, 1km; NHM1km, 250 m; NHM250m; 50 m; NHM50 m) were used. The vertical coordinate is terrain-following and contains 50 levels with variable grid intervals of $\Delta z = 40$ m near the surface to 904 m at the top (NHM1km and NHM250m), and 90 levels with $\Delta z = 40$ m to 304 m (NHM50m). The initial and boundary conditions of NHM5km are provided from the operational regional analysis of JMA.

3. Simulated environmental fields around the outer rainband

NHM1km reproduced the outer rainband about 300 km away from the typhoon center in the right-front quadrant of translating Shanshan. The wind hodograph around the rainband shows that the strong vertical shear with veering existed below 2 km AGL. The distribution of storm-relative helicity shows the peak with more than $750 \text{ m}^2 \text{ s}^{-2}$ but that of CAPE is not related to the location of the rainband.

4. Simulated mini-supercell structure by the NHM250m

Figure 1a presents the simulated rainband by the NHM250m. The rainband consists of a number of isolated active convective cells. Some convective cells have the hook pattern and bounded weak region of hydrometeors at the southern tip of them (Fig. 1b). The maximum vertical vorticity is about $7 \times 10^{-2} \text{ s}^{-1}$ and upward motion is more than 30 m s^{-1} around 1 km and 3 km above AGL (Fig. 1c). The vertical and horizontal scale is small compared to the typical supercell storm over the Great Plains of the United States. These features are identical to the mini-supercell as showed in many previous studies (eg., Suzuki et al. 2000). Another noteworthy feature is that the gust font near the surface boundary is distinguishable by the wind field and vertical vorticity, however, the horizontal gradient of temperature across it is weak. As this storm approached the land, the mesovortices at low-level intensified significantly.

5. Simulated tornado structure by the NHM50m

Figures 2a and 2b show the successfully simulated tornado spawned by the mini-supercell noted above. Note that this simulation includes full-physics processes and free-slip surface condition is not used unlike the other previous studies. The tornado was generated on the gust front and moved with the rapid translation speed of about 100 km h^{-1} over the sea. The vertical vorticity reached 0.7 s^{-1} and surface pressure drop was about 12 hPa. The diameter of the vortex near the surface is about 500 m. The tornado exhibited the asymmetric structure with strong winds of more than 50 m s^{-1} only on the right side and tilted northwestward vertically.

Further analytical and numerical studies are being conducted focusing on the evolution of the mini-supercell storm and the tornadogenesis process.

Acknowledgments

The author would like to thank T. Kato, S. Hayashi and N. Seino of the MRI/JMA for their support to conduct the numerical simulation.

REFERENCES

- Saito, K., T. Fujita, Y. Yamada, J. Ishida, Y. Kumagai, K. Aranami, S. Ohmori, R. Nagasawa, S. Kumagai, C. Muroi, T. Kato, H. Eito, and Y. Yamazaki, 2006: The operational JMA nonhydrostatic mesoscale model. *Mon. Wea. Rev.*, 134, 1266-1298.
- Suzuki, O., H. Niino, H. Ohno, and H. Nirasawa, 2000: Tornado-producing mini supercells associated with Typhoon 9019. *Mon. Wea. Rev.*, 128, 1868-1882.

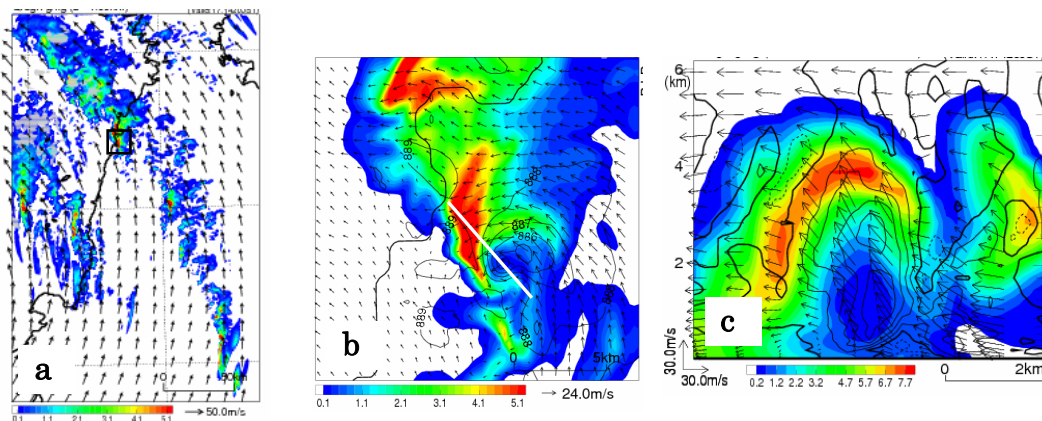


Fig. 1. (a) Horizontal distribution of hydrometeors and wind vectors at a height of 1 km by NHM250m. (b) Enlarged illustration of the square box in (a). Contour lines denote the pressure with 1 hPa interval. Arrows show the storm-relative wind. (c) Vertical cross section along the line in (b). Contour lines denote vertical vorticity with 0.015 s^{-1} interval.

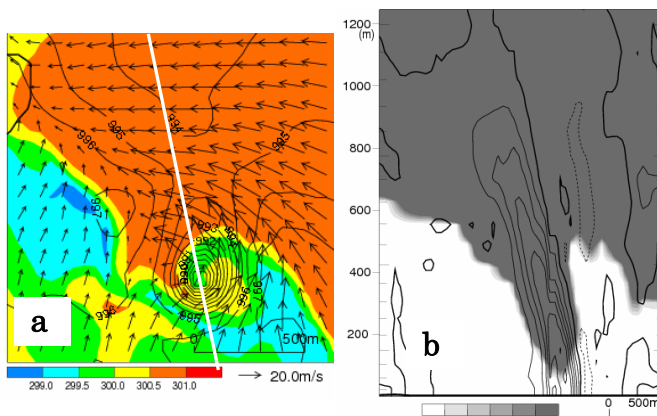


Fig. 2. Simulated tornado structure by NHM50m. (a) Potential temperature with the wind vectors at 20 m AGL. Contour lines denote the surface pressure with 1 hPa interval. (b) Vertical cross section of cloud water along the line in (a). Contour lines denote vertical vorticity with 0.1 s^{-1} interval.

Precipitation Efficiency in Numerically Simulated Orographic Rainfall Associated with Typhoon Meari (2004)

Akihiko MURATA

Meteorological Research Institute / Japan Meteorological Agency, Tsukuba, Ibaraki 305-0052, Japan
(corresponding author: amurata@mri-jma.go.jp)

1. Introduction

Precipitation efficiency in numerically simulated orographic rainfall has been investigated using a nonhydrostatic model. The targeted area was the east coast of the mountainous Kii peninsula, Japan, same as Murata (2006), refereed to as M2006. The study demonstrated that three characteristic precipitation systems affect the 12-h accumulated rainfall between 0300 Japan Standard Time (JST) and 1500 JST 29 September 2004. The period includes the heaviest rainfall, more than 100 mm/h, at Owase, located at the middle part of the east coast of the peninsula.

In the present study, on the basis of the results of the high-resolution nonhydrostatic simulations, precipitation efficiency is investigated in order to clarify the mechanisms of the heavy rainfall.

2. Numerical model and experimental design

The numerical model we used was the Japan Meteorological Agency Nonhydrostatic Model (JMANHM; Saito et al., 2006) with the horizontal grid spacing of 1 km and 5 km (referred to 1 km-NHM and 5 km-NHM, respectively). We adopt a grid-nesting strategy for the initial and lateral boundary conditions: double nested JMANHM. The nesting procedure is as follows: The initial (2200 JST 28 September 2004) and lateral boundary data for 1 km-NHM (501×501×50 grid points) were obtained from forecasts produced by 5 km-NHM (719×575×50 grid points). The initial (2100 JST 28 September 2004) and lateral boundary data for 5 km-NHM were obtained from the JMA mesoscale analysis data produced with a four-dimensional variational assimilation technique. Kain-Fritsch convection scheme was included in 5 km-NHM in addition to a bulk cloud microphysical scheme.

3. Results

It is desirable to understand the efficiency of a heavy-rainfall event for clarifying the mechanisms of the event. A measure for this purpose is called precipitation efficiency, defined as the ratio of the surface rainfall rate to moisture convergence, or to the sum of condensation and deposition. Market et al. (2003) reviewed previous studies on precipitation efficiency and summarized the precipitation-efficiency values derived from previous studies. Whereas many observational studies have been conducted on precipitation efficiency (e.g., Rauber et al. 1996), few modeling studies have discussed issues related to precipitation efficiency (e.g., Ferrier et al. 1996).

The time series of variables, regarding precipitation, horizontally averaged over a 60-km square centered on Owase are shown in Fig. 1. The variables include water vapor flux convergence, the sum of condensation and deposition, and precipitation, where the former two are vertically integrated variables and the latter is the variable observed at the surface. The period shown in Fig. 1 is divided into three periods: 1) 0300-0600 JST, 2) 0600-0900 JST, and 3) 0900-1200 JST. The first period (0300-0600 JST) corresponds to that when only the precipitation system A of M2006 affects the variables. In the third period (0900-1200 JST), on the other hand, the variables are influenced by all precipitation systems (i.e., A, B, and C of M2006). In contrast, the effects of the systems seem to be less in the second period (0600-0900 JST).

Precipitation efficiency (PE) here is defined to be the amount of rainfall reaching the ground divided by the sum of vertically accumulated condensation and deposition. Other two efficiencies are defined as follows: 1) Condensation efficiency (CE): The sum of vertically accumulated condensation and deposition divided by vertically accumulated water vapor flux convergence, and 2) Multiplied efficiency (ME): The amount of rainfall reaching the ground divided by vertically accumulated water

vapor flux convergence. ME therefore is the product of CE and PE.

It is found that PE has the largest value in the period of the heaviest precipitation, leading to the largest values in ME. The calculation of the efficiencies in each period mentioned above shows PE in the third period is larger than that in the first period, although CEs in the two periods are not so different (Fig. 2). The difference in ME between the two periods is attributed to that in PE.

The larger PE suggests that some cloud microphysical processes efficiently produce rainwater. Detailed examination of the production terms for rainwater revealed that accretion of cloud water by rainwater is primarily responsible for the total production of rainwater. It was also found that the accretion term has the largest values in the third period compared with those in the other two periods. The largest values in the accretion term during the heaviest rainfall period are probably attributed to deeper layer of cloud water, compared with those in the other periods. The depth depends on the vertical structure of the precipitation systems. The system C of M2006 is characterized by a structure similar to the primary rainband in a tropical cyclone and consists of deep convective clouds.

Acknowledgements

The author acknowledges T. Kato and S. Hayashi of the MRI / JMA for developing computer codes for nesting.

References

- Ferrier, B. S., J. Simpson, and W.-K. Tao, 1996: Factors responsible for precipitation efficiencies in midlatitude and tropical squall simulations. *Mon. Wea. Rev.*, 124, 2100-2125.
- Market, P., S. Allen, R. Scofield, R. Kuligowski, A. Gruber, 2003: Precipitation efficiency of warm-season midwestern mesoscale convective systems. *Wea. Forecasting*, 18, 1273-1285.
- Murata, A., 2006: A cloud-resolving numerical simulation for orographic rainfall associated with typhoon Meari (2004). *CAS/JSC WGNE Res. Activities in Atm. and Oceanic Modelling*, No. 36. 5.37-5.38.
- Rauber, R. M., N. F. Laird, and H. T. Ochs III, 1996: Precipitation efficiency of trade wind clouds over the north central tropical Pacific Ocean. *J. Geophys. Res.*, 101, 26247-26253.
- Saito, K., T. Fujita, Y. Yamada, J. Ishida, Y. Kumagai, K. Aranami, S. Ohmori, R. Nagasawa, S. Kumagai, C. Muroi, T. Kato, H. Eito and Y. Yamazaki, 2006: The operational JMA Nonhydrostatic Mesoscale Model. *Mon. Wea. Rev.*, 134, 1266-1298.

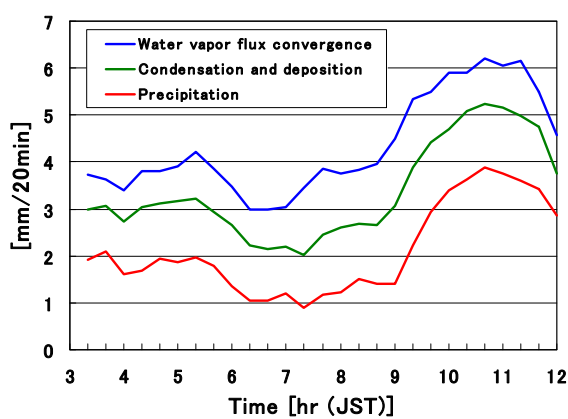


Fig.1 Time series of precipitation, the sum of condensation and deposition, and water vapor flux convergence.

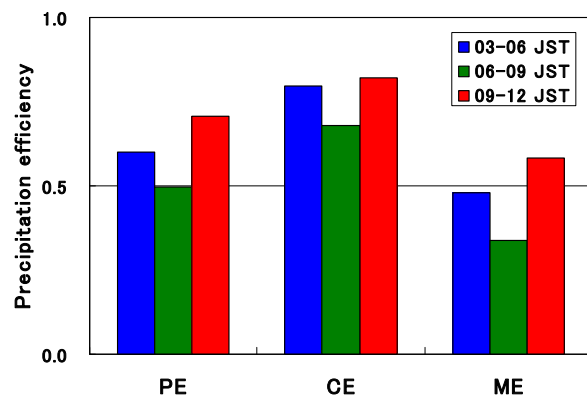


Fig.2 Precipitation efficiency, condensation efficiency, and multiplied efficiency for each periods.

Experimental operation of a high-resolution local forecast model at JMA

Hiroshi Nakayama, Yoshihiro Ishikawa, Tadashi Fujita and Kensuke Takenouchi
Numerical Prediction Division, Japan Meteorological Agency,
1-3-4 Otemachi, Chiyoda-ku, Tokyo 100-8122, Japan
E-mail: h-nakayama@met.kishou.go.jp

1. Introduction

The Japan Meteorological Agency (JMA) operates the meso-scale model (MSM) whose horizontal grid spacing is 5 km. In addition, a high-resolution local forecast model (LFM), whose horizontal grid spacing is 2 km, has been developed to provide more detailed information for disaster prevention and aviation safety. The LFM is planned to be operational in 2011 or later.

An experimental run of the LFM has been executed 3-hourly (8 times a day) since 1 June 2006 with a much smaller domain than that of planned operation.

This paper describes the specification and the results of this experimental run.

2. Specifications of the experimental LFM

The LFM has been developed based on the JMA nonhydrostatic model (Saito et al. 2006).

For its initial condition, a 3-dimensional variational (3DVAR) version of JNoVA (JMA Non-hydrostatic Model based Variational Data Assimilation System) is employed. And its boundary field is prepared from the operational MSM which runs every 3-hourly.

The initialization and the forecast of the experimental run are as follows (Fig.1). As the first step, the JNoVA-3DVAR is executed with 5km grid spacing using 3-hour forecast of the operational MSM as a first guess field, and the MSM is executed for 1 hour with a smaller domain than operational one (Fig.2). Then, a rapid update cycle is materialized through

both the JNoVA-3DVAR and the MSM. In this assimilation, the assimilated data are wind and temperature observational data of AMeDAS¹, WINDAS², ACARS³, Doppler radar, all of which are suitable instruments to capture mesoscale phenomena.

The forecast domain of the experimental LFM is Kanto area with 151 x 151 grid points (Fig.2).

The specifications of the experimental LFM and the operational MSM are summarized in Table 1.

3. Verification results

In this section, the results of the experimental LFM are shown in terms of statistical verification scores in comparison to the operational MSM for the period from June to December in 2006.

The forecasted precipitation is verified against the Radar-Raingauge Analyzed Precipitation data. The verifications were carried out for every 20 km square mesh over land and sea near the coast. Fig 3 shows the bias (BS) and the equitable threat scores (ETS) of a mean and a maximum value in each mesh about one-hour precipitation forecast by the LFM and the MSM. The BS of the mean of the LFM shows more excess of precipitation area for heavier rain. The ETS in the mean of the LFM shows insufficiency of weak rain forecast. In contrast, the BS in the maximum of the LFM is closer to unity than that of the MSM. The ETS in maximum of the LFM is better than that of the MSM except weak rain. These results show that the LFM is able to forecast the peaks of heavy rain well.

Fig 2 shows the mean error (ME) and root

Table 1. the Specifications of the operational MSM and the experimental LFM.

| | MSM | LFM |
|------------------------------|------------------------------|-----------------|
| Horizontal mesh (resolution) | 721 x 577 (5km) | 151 x 151 (2km) |
| Forecast period | 15 hours | 12 hours |
| Initial conditions | Meso 4DVar | JNoVA-3DVar |
| Lateral boundary | RSM* | MSM |
| Levels | 50 | 60 |
| Moist physics | 3 ice bulk microphysics | Same as in MSM |
| Convection | Modified Kain-Fritsch scheme | None |

* Regional Spectral Model

¹ AMeDAS(Automated Meteorological Data Acquisition System) is a high-density surface observation network covering Japan.

² WINDAS(Wind Profiler Network and Data Acquisition System) is covering Japan with spatial resolution of 130 km on the average.

³ ACARS(Aircraft Communications Addressing and Reporting System) reports weather information from aircrafts.

mean square error (RMSE) of the surface temperature and wind forecast by the LFM and the MSM against the AMeDAS data of about 80 points in the domain. On surface temperature, both the ME and the RMSE of the LFM are better all day than those of the operational MSM, but the LFM has a negative bias in day time. On surface wind speed, both the ME and the RMSE of the LFM are almost same as those of the MSM.

Reference

Saito, K., T. Fujita, Y. Yamada, J. Ishida, Y. Kumagai, K. Aranami, S. Ohmori, R. Nagasawa, S. Kumagai, C. Muroi, T. Kato and H. Eito, 2006: The operational JMA Nonhydrostatic Mesoscale Model. Mon. Wea. Rev., 134, 1266-1298.

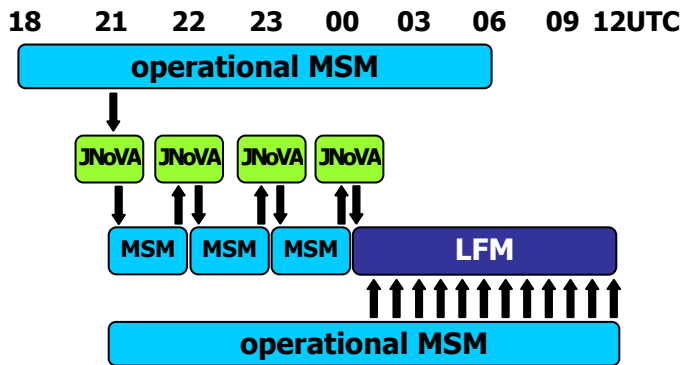


Fig 1. Initialization and Nesting procedure

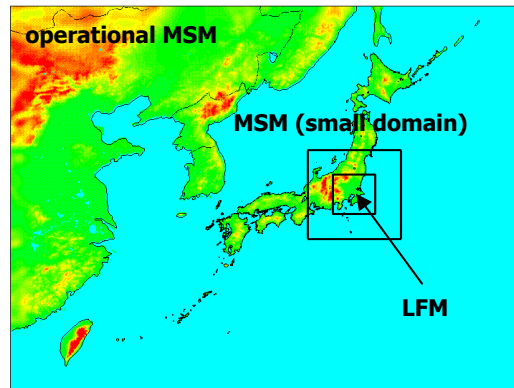


Fig 2. The Domain of models.

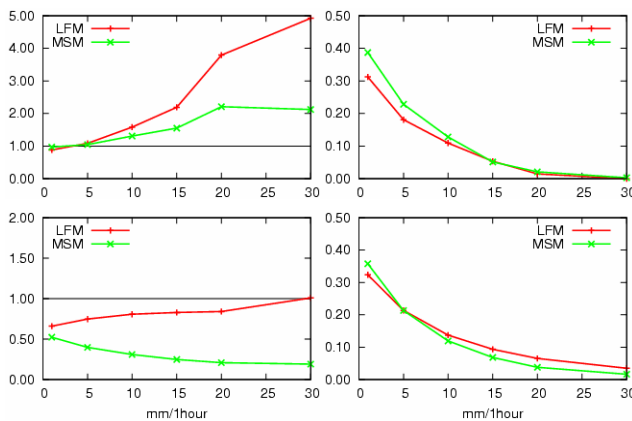


Fig 3. The bias and equitable threat scores of precipitation forecast against R-A (Radar-Raingauge Analyzed Precipitation). The red line indicates the LFM and the green line indicates the operational MSM. left : bias score, right : equitable threat score, upper : average , lower : maximum in every 20 km square mesh over land and over sea near the coast.

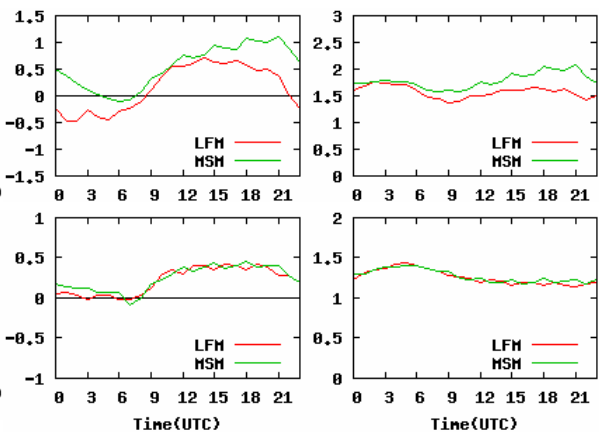


Fig 4. The Diurnal Change of mean errors (ME) and root mean square errors (RMSE) of temperature and wind speed (03 UTC is noon and 15 UTC is midnight at local time). The red line indicates the LFM and the green line indicates the operational MSM. left: ME, right: RMSE, upper: temperature, lower: wind speed.

Calculation of the tracks of typhoons threatening the coasts of Russia

A.E. Pokhil, A.D. Naumov, M.Yu. Zaichenko

Russian Hydrometeorological Research Center, 9-11, Big Predtechensry lane, 123242, Moscow, Russia, pokhil@mecom.ru

The typhoon Nabi, the 14th tropical cyclone (TC) moving in the northwest of the Pacific in 2005, originated on 29 August at 14.5° N, 154° W and reached the typhoon stage on the 1st of September. It was supposed that it would make landfall on the island Hokkaido, would cover the south of Sakhalin, then the South Kurile Islands and would reach Kamchatka. The cities of Russia in the coastal zone of said territories would have been threatened with storm winds, showers and a huge storm wave.

In the Hydrometeorological Center of Russia, in the laboratory of the dynamics of the atmosphere in the tropical zone of the World Ocean, the calculations of the motion and evolution of the TC were made on the basis of the regional ETA model.

The model is adapted for the global data of the Hydrometeorological Center of Russia. As a result a technology has been created that makes it possible to take the data of the objective analysis of the Hydrometeorological Center of Russia and the forecasts using the spectral model of the Hydrometeorological Center as the input data for the ETA model.

The input data for the ETA model are the fields of the geopotential, of the zonal and meridional components of the wind velocity, of temperature on 10 standard isobaric surfaces (1000 – 100 hPa). Initial data and lateral boundary conditions are taken every 6 h from operative analyses of ECMWF that were not subject to initialization. The model version used in the Hydrometeorological Center includes extra blocks responsible for the TC motion and strength.

Presently the mentioned technology enables us to make forecasts of fields of meteorological values over vast territories for the periods up to 48 h on the basis of the on-line data available in the Hydrometeorological Centre of Russia, to make calculations characterizing the forecasts verification score etc.

What is important, the ETA model designed for the forecast general purposes operates within the framework of a developed prognostic system implying not only the release of operative forecasts using this model, but also all the procedures associated with the collection, preliminary processing (pre-processing) of the input information, interpretation of the output information (post-processing). The system implies also tackling the problem of the dissemination of the prognostic data obtained using the above-mentioned) model, and the problem of creation of the database and archives.

The goal was building a certain “sub-system” meant for the TC operative forecasting achieving the stage of visualization of the calculated forecasts of both TCs themselves and the large-scale fields surrounding them.

The calculation of the tracks and the evolution of tropical cyclones is performed on the basis of the solution of a system of hydrodynamic equations, in incremental representation, with a horizontal step of 30 km and with 32 levels vertically. In the course of integration and tracking of the cyclone the point with the local maximum in the vorticity field is took as (/is assumed to be) the cyclone center.

In the problem under consideration the integration region is 116 - 164° E, 10 - 50° N. For the initial data the data of the on-line analysis and of real-time forecast made in the Hydrometeorological Centre of Russia for 00 UTC for 6 August 2001, as well as those of the re-analysis were taken.

The trajectory of Nabi was of parabolic character. The TC reached its utmost strength ($P = 925$ hPa, $V = 42$ m/s) on 2 September, in the open ocean. On 6 September the TC made landfall on the western coast of the island Kyushu and, further, moved in the Sea of Japan.

To estimate what threat the typhoon Nabi constituted to the Russian littoral, a forecast of the TC Nabi motion was performed using the ETA model for 2 days beginning from 6 August.

The results of the calculation have shown that in 24 hours from the beginning of the calculation, i.e. at 00 UTC 7 September, Nabi should have been located in the southern part of the Sea of Japan (37° N, 133° E) (actually its center turned out to be in the point 37.8° N, 134.6° E), and that within the following 24 hours it would move towards the island Hokkaido and further cover the South Kuril Islands (the island Kunashir and the island Shikotan). The coordinates of the calculated point of the TC center location are 43.5° N, 142° E (the actual one was located at 44° N, 144.5° E).

The comparison of the analysis fields built at the Hydrometcentre of Russia (Department of Global Analysis and Forecast of Weather) with the analysis and forecast of pressure fields based on the calculation using the ETA model shows that the latter ones do not rank below (as for the precision of the description of the real situation in the aquatory occupied by the TC) the analysis of the situation made on the basis of international data. The forecast of the mentioned fields for 24 and 48 h is close to the real situation.

A high resolution, real time experimental forecast for the Río de la Plata: A “Sea-Breeze” case study.

Juan Ruiz

Centro de Investigaciones del Mar y la Atmósfera, Departamento de Ciencias de la Atmósfera y los Océanos, Facultad de Ciencias Exactas y Naturales, Universidad de Buenos Aires, Argentina.

jruiz@cima.fcen.uba.ar

1. Introduction:

The Río de la Plata is one of the largest estuaries in the world and is located at the opening of the Paraná river between Argentina and Uruguay. Due to its large extent, the differential diurnal cycle of heating between the estuary and the shores forces local circulations (Berri and Nuñez 1993, Berri and Straibman, 2005) which affect both sides of the shores. This kind of effect is important to sport navigation, transport of pollutant agents while it can also produce significant changes in temperature and moisture over the shores, with circulations penetrating more than 70 km inland. Sometimes under unstable conditions, convergence associated with these local circulations can trigger thunderstorms.

The Advanced Research WRF (Weather Research and Forecasting) (Skamrok, 2005) has been used in idealized studies to simulate local circulations like mountain-valley breezes (Rampanelli et. al. 2004). It has also been tested for real time experimental forecasts with resolutions as high as 4 km over the United States with a focus on the forecast of convection (<http://rain.mmm.ucar.edu/wrf/>). In this work the WRF-ARW is used in an experimental real time forecast of the “Sea Breeze” effect over the Río de la Plata. The 9th December 2006 case has been selected to preliminary assess model performance.

2. Methodology:

In order to simulate the local circulations associated with temperature gradients along the shore, the WRF-ARW model has been run covering the entire estuary (Fig. 1 a) with a horizontal resolution of 5 km and 36 vertical levels between the surface and 500 hPa., given that the focus of the experiments is in the low level circulation. The model has been run with moisture treated as a passive tracer to avoid the generation of other local circulations associated with latent heating or cold pools development, and to reduce computational cost. Future experiments will include the effects of rain and clouds which are very important for an operational implementation.

The initial conditions for the model are taken from the GFS-NCEP (Global Forecasting System- National Centre for Environmental Prediction) analysis. The boundary conditions are provided at 3 hour intervals by the WRF-ARW real time forecast performed twice a day at CIMA (Centro de Investigaciones del Mar y de la Atmósfera) with a horizontal resolution of 20 km.

The 9th December 2006 “sea breeze” event selected for this case is particularly suitable due to the small amount of cloud cover over the domain, what reduces the potential impact of running the model in a no-precipitation mode. Doppler radar data and surface observations provided by the National Weather Service of Argentina are used to compare the observed local circulation with that forecasted by the model.

3. Results:

During the early morning, on December 9 2006, a weak trough associated with low level convergence crossed over the model domain and after that, the circulation in the Argentinian shore was dominated by weak winds from the southwest (less than 10 km/h) (Fig 1 b). During the daytime a local circulation due to differential heating established along the Argentinian shore, as denoted by the wind rotation at Aeroparque station (see fig. 1 b for station location) that goes from the SW to the E at noon (15 UTC) and then to the NE.

Around 18 UTC a well developed land-sea breeze front is indicated by a narrow band of weak reflectivity in the RADAR located at Ezeiza (Figure 2 a). The doppler velocity also indicates a wind shift associated with this sea-breeze front (not shown). Figure 2 b, shows the WRF-ARW experimental forecast verifying at the same hour, with a well developed and correctly positioned wind shift line. Strong low level convergence also develops along the shore (Figure 2 b) co-located with the upward branch of the sea-breeze circulation (not shown). Areas of low level divergence developed over the estuary associated with broad subsidence over the area. Figure 3 shows the wind direction for Aeroparque (Figure 3 a) and Ezeiza (Figure 3 b). The wind shift associated with the breeze circulation is well reproduced by the model at both stations although the change in direction takes place earlier in the model than in the observations.

These results are encouraging and suggest that an operational forecast of local circulations over the Río de la Plata is possible provided a good regional forecast is available. Cloud and precipitation effects as well as an increased vertical coverage should be included in future experiments to better represent events where convection could have a prominent role.

4. Acknowledgments: This research is sponsored by the Research Grant PIP 5417 CONICET (Consejo Nacional de Investigaciones Científicas y Técnicas).

5. References:

- Berri, G. J. and M. N. Nuñez: **Transformed Shoreline-following Horizontal Coordinates in a Mesoscale Model: A Sea-Land-Breeze Case Study**; *Journal of Applied Meteorology*. Vol 32, pp. 918-928.
- Berri, G. J. and L. Straibman: **Low level atmospheric circulation simulated with a boundary layer numerical model forced with regional mean conditions: exploratory analysis over the Río de la Plata**, 2005 (in Spanish) presented at CONGREMET IX, Buenos Aires, Argentina.
- Rampanelli, G. D. Zardi and R. Rotunno: **Mechanisms of Up-Valley Winds**: 2004, *Journal of the Atmospheric Sciences*. Vol 61, pp. 3097-3111.

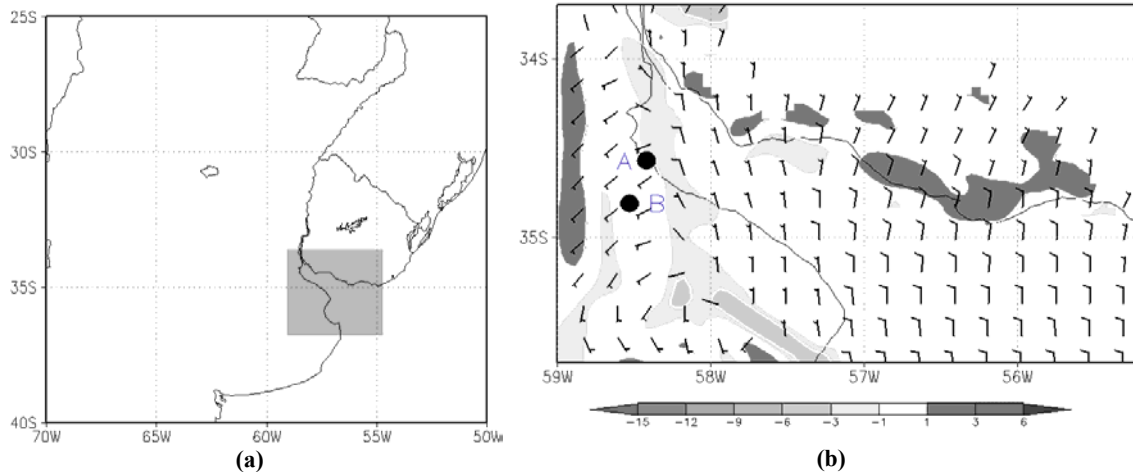


Figure 1: (a) Domain location (gray rectangle) and (b) 30 hour forecast verifying at 06 UTC 9th December 2006. Wind barsbs at 100 meters ($m s^{-1}$) and convergence (shaded) ($1e 4 s^{-1}$). The black circles in the Argentinian shore indicate the position of Aeroparque (A) and Ezeiza (B) stations.

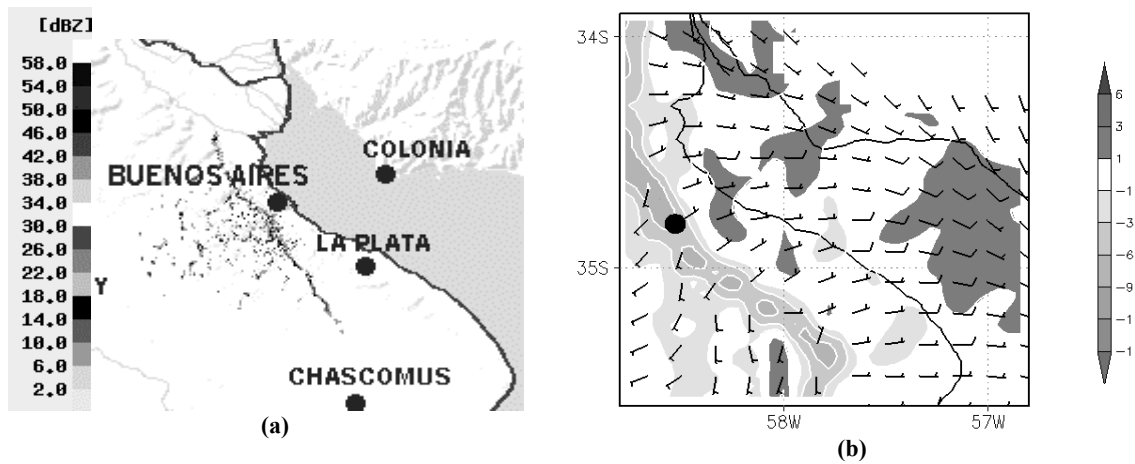


Figure 2: (a) Radar reflectivity (shaded) (dBz). (b) as in Figure 1 but for a smaller region. The black circle represents the location of the Radar. Both at 21 UTC 9th December 2006.

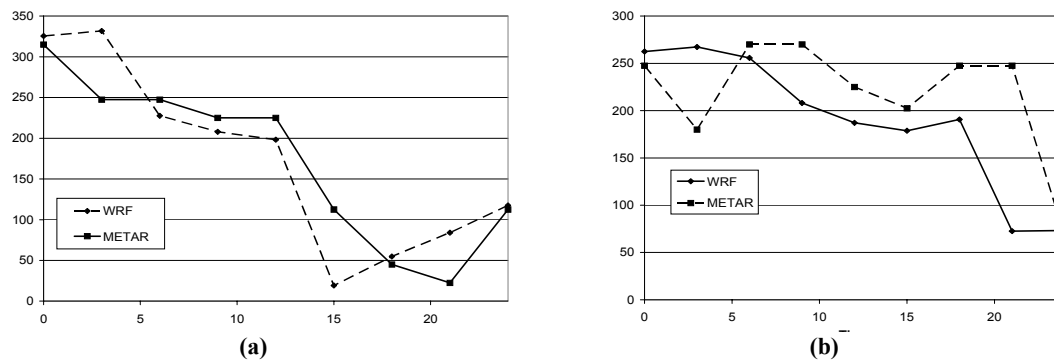


Figure 3: Wind direction (degrees) forecasted by the WRF model (dashed) and observed (solid line) between 00 UTC 9th and 00 UTC 10th December 2006. For (a) Aeroparque and (b) Ezeiza.

Preliminary Mesoscale Ensemble Prediction experiment for WWRP Beijing 2008 RDP

Kazuo Saito*, Hiromu Seko*, Masaru Kunii*

Tabito Hara**, Masayuki Kyouda** and Munehiko Yamaguchi**

* Meteorological Research Institute, Tsukuba, Ibaraki 305-0052, Japan; ksaito@mri-jma.go.jp

** Numerical Prediction Division, Japan Meteorological Agency

The WWRP Beijing 2008 Forecast Demonstration / Research and Development Project (B08FDP/RDP) is an international research project for a short range forecast of the WMO World Weather Research Programme, which succeeds the Sydney Olympic 2000 Forecast Demonstration Project (Sydney 2000FDP). The B08FDP/RDP is divided into two components; the FDP component for a very short range forecast up to 6 hours based on the nowcasting, and the RDP component for a short range forecast up to 36 hours based on the mesoscale ensemble prediction system (MEPS). Collaborating with JMA, the Meteorological Research Institute (MRI) proposed its participation in the RDP component at the 1st WWRP B08 workshop held in 2005.

A preliminary test for B08RDP was performed for 8-24 August 2006 by five participant centers including MRI/JMA, NCEP, Meteorological Service of Canada, China Meteorological Administration and the Chinese Academy of Meteorological Sciences (CAMS). Main purposes of this test were construction of basic systems for MEPS and check of the data transfer. In the Tier 1 experiment, mesoscale ensemble predictions with a horizontal resolution of 15 km were conducted, and surface level data (2m temperature, 2m relative humidity, 10m winds, MSL pressure and 3 hour accumulated rain) at uniform 0.15 degree common grids for a domain of 105°E-125°E, 30°N-45°N were transferred to CMA in the GRIB2 format.

MRI/JMA conducted 11 member meso-ensemble predictions with the JMA nonhydrostatic model (Saito et al., 2006a) which covers a domain of 3300 km x 3000 km (Fig. 1). This domain is slightly smaller than the recommended area in B08RDP (3500 km x 3000 km) and the southwestern corner of the verification domain is embedded in boundary relaxation layers (24 grids = 360 km).

Specifications of the experimental design are listed in Table. 1. Except horizontal resolution and domain size, most of them are same as in the JMA operational mesoscale model. Initial condition of the control run is given by the JMA operational regional analysis, while for the initial perturbations for ensemble members, perturbations from the JMA operational one week global EPS are employed after an appropriate normalization as in Saito et al. (2006b). Examples of the ensemble forecasts for a case of 15 August 2006 are shown in Fig. 2.

Figure 3 shows 24 hour forecast RMSEs of the control runs and the ensemble mean forecasts against the initial condition over the common verification domain. In all cases, RMSEs of the ensemble mean forecasts are smaller than those of control runs. Similar tendencies are obtained for horizontal wind, relative humidity and precipitation. Figure 4 indicates time sequences of the ensemble spreads during the verification period. Spreads of horizontal winds (U and V) increase up to FT=27, while the spread of MSL pressure slightly decreases after FT=7. These tendencies are attributable to the lateral boundary condition without perturbation. Compared with the forecast errors in Fig. 3, the forecast spreads are not necessarily large enough. Inclusion of perturbations in lateral boundary conditions as well as the alternative ways to give the initial perturbations are our next subjects. Developments of BGM and SV methods using JMA-NHM are underway.

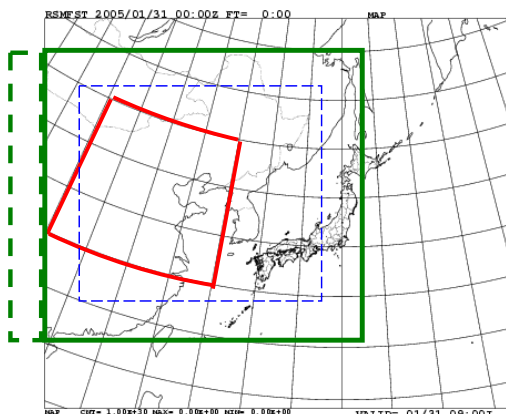


Fig. 1. Domain of the MRI/JMA preliminary experiment (solid rectangle). Fan-shaped sector over east China indicates the domain of 0.15 degree common verification grids (105°E-125°E, 30°N-45°N). Broken lines show the boundary relaxation area. Broken rectangle left of the model domain shows the size of the recommended domain.

Table 1. Specifications of the preliminary MEP experiment by MRI/JMA.

| | |
|-----------------------------------|---|
| Forecast time (number of members) | 36 hours (11 members) |
| Horizontal resolution (grid size) | $\Delta x=15\text{km}$ (221 \times 201) , Lambert conformal |
| Vertical levels | 40 levels, $\Delta z=40\text{-}1180$ m |
| Initial condition for control run | JMA operational Regional analysis |
| Initial perturbation | JMA operational one week global EPS (normalized) |
| Lateral boundary condition | JMA operational Regional model 3 hourly (no perturbation) |
| Dynamics | HE-VI scheme, $\Delta t=60$ sec, $\Delta \tau=17$ sec |
| Cloud microphysics | 3 ice bulk method |
| Convective parameterization | Modified Kain-Fritsch scheme |
| Turbulence | Diagnostic TKE |
| Ground temperature | Prognostic 4 soil levels (no initial perturbations) |

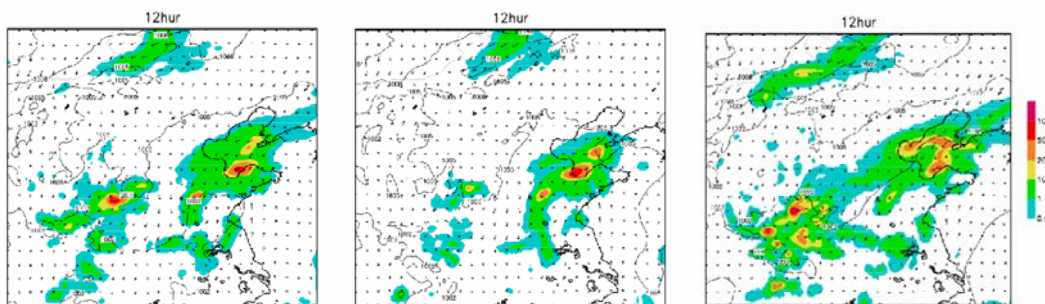


Fig. 2. 3 hour accumulated rain for 12 hour forecast of JMA-NHM with the control run (Left), member M02p (center), and member M02m (Right). Initial time is 12 UTC 14 August 2006.

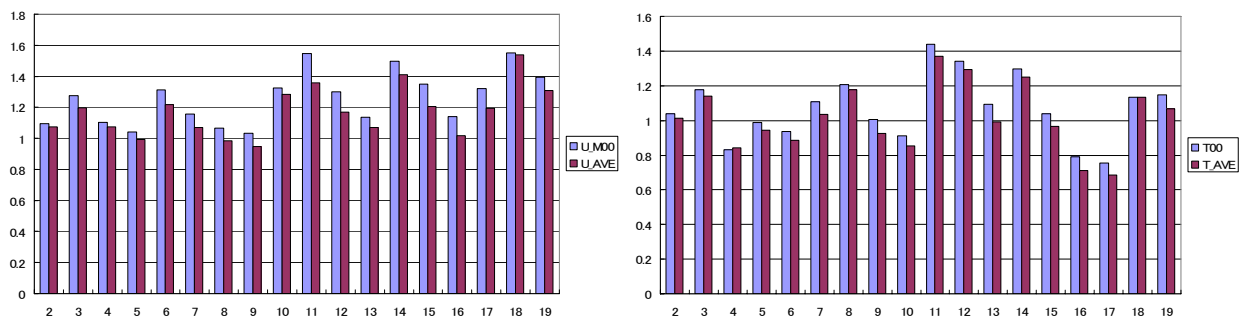


Fig. 3. 24 hour forecast RMSEs of the control run and the ensemble mean against initial condition over the verification domain. Verification period is 18 days from 2 to 19 August. Left) 10 m wind (U). Right) 2 m temperature.

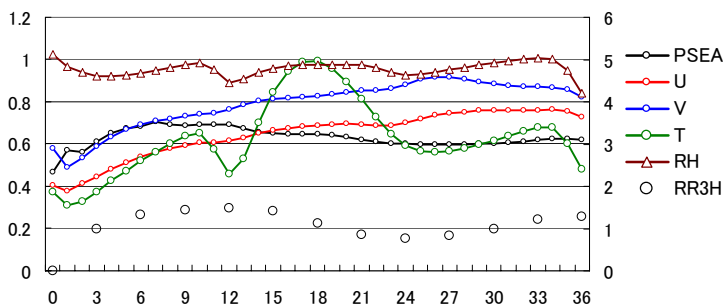


Fig. 4. Time sequences of the ensemble spreads. Unit of the left vertical axis is ‘hPa’ for MSL pressure (PSEA), ‘m/s’ for horizontal winds (U and V), ‘K’ for 2m temperature (T), respectively. Unit of the right vertical axis is ‘%’ for relative humidity (RH) and ‘mm’ for 3 hour accumulated rain (RR3H), respectively.

References

- Saito, K., T. Fujita, Y. Yamada, J. Ishida, Y. Kumagai, K. Aranami, S. Ohmori, R. Nagasawa, S. Tanaka, C. Muroi, T. Kato and H. Eito, 2006a: The operational JMA nonhydrostatic mesoscale model. *Mon. Wea. Rev.*, **134**, 1266-1298.
- Saito, K. M. Kyouda and M. Yamaguchi, 2006b: Mesoscale Ensemble Prediction Experiment of a Heavy Rain Event with the JMA Mesoscale Model. *CAS/JSC WGNE Research Activities in Atmospheric and Oceanic Modelling*. **36**, 5.49-5.50.

Development of a BGM method with the JMA nonhydrostatic mesoscale model

Kazuo Saito

Meteorological Research Institute, Tsukuba, Ibaraki 305-0052, Japan; ksaito@mri-jma.go.jp

In the previous report (Saito et al., 2006a), we conducted a mesoscale ensemble prediction experiment for a case of the 2004 Niigata heavy rain where initial perturbations of the ensemble members were given by normalized perturbations from the JMA operational one week ensemble prediction system (global EPS). Downscaling of global EPS is one of the promising methods, which offers detailed scenarios of mesoscale phenomena corresponding to possible synoptic situations. However, the operational global EPS is designed for the one week forecast so that the initial perturbations are adjusted to obtain appropriate spread of the synoptic fields. Therefore, the initial perturbations of the global EPS are not necessarily best for mesoscale prediction. Indeed, in Saito et al (2006a), though some perturbed members succeeded to predict a band-shaped intense rainfall area in the later half of the forecast period, rainfall amounts of ensemble members varied widely in the initial stage.

The breeding mode (BGM) method is a typical way to produce initial perturbations in the ensemble prediction. It selectively raises the Lyapunov vectors in the breeding cycle and is widely used in several operational EPSs including the JMA global EPS and the NCEP's Short Range Ensemble Forecast (SREF) system. Development of a BGM method which employs the self breeding cycle with the JMA mesoscale model is underway.

A self breeding cycle has been constructed using the JMA nonhydrostatic model (JMA-NHM). Specifications of the experiment are listed in Table. 1. The domain and resolutions are same that of the JMA operational mesoscale model (Saito et al., 2006b), while the horizontal resolution of the JMA operational model has been enhanced to 5 km since March 2006. To evaluate the magnitude of the bred perturbations, the moist total energy norm by Barkmeijer et al. (2001),

$$TE = \frac{1}{2} \iint \{ (U_p - U_c)^2 + (V_p - V_c)^2 \} + \left\{ \frac{c_p}{\Theta} (\theta_p - \theta_c)^2 \right\} + w_q \frac{L^2}{c_p \Theta} (q_p - q_c)^2 dS dP$$

$$+ \frac{1}{2} \int \left\{ \frac{R\Theta}{P_r} (P_{seaP} - P_{seaC})^2 \right\} dS,$$

is employed. Here, according to the JMA global EPS, the values of $\Theta = 300$ K, $P_r = 800$ hPa and $w_q = 0.1$ are used and the norm is computed less than 5.3 km AGL height. Targeting the 2004 Niigata heavy rain event, 12 hourly twelve self breeding cycles are conducted from 12 UTC 09 July to 12 UTC 12 July 2004. The moist total energy norms are computed by the differences between the control runs and perturbed runs, and the bred perturbations of all prognostic variables except soil temperatures are normalized 12 hourly. The normalization coefficients are determined by the square root of ratios between the total energy norms of perturbed runs and a standard norm, which is computed by prescribed values of model variables (0.35 hPa for MSL pressure, 1.0 m/s for U and V , 0.4 K for θ and 5 % for relative humidity, respectively). In 18 hour forecasts from 12 UTC 12 July, initial conditions of 24 members are given by 12 sets of positive and negative perturbations which are normalized twice to the breeding cycle. In the perturbed initial conditions, mixing ratio of the water vapor is limited by the saturation mixing ratio.

Figure 1 shows 6 hour accumulated rain over northern Japan (rectangle in Fig. 3a) in case initial perturbations are given by the global EPS. In both averaged and peak values, rainfall amounts of ensemble members varies widely in the initial stage (FT=0-6). Figure 2 shows the corresponding result where initial perturbations are given by the BGM method. The variation of rainfall amount in initial stage is reduced, which means that the initial perturbations are more appropriate for mesoscale prediction. In the later half of the forecast period (FT=12-18), the variety of precipitation amount reaches 2 times in averaged values and 3 times in peak values. Figure 3 shows simulated 3 hour rainfall in member 'M03p' at FT=18 for BGM method. A band-shaped intense rainfall area similar to observation is predicted.

Table 1. Specifications of the preliminary BGM experiment.

| | |
|-----------------------------------|---|
| Breeding cycle | 12 hours (5 members) |
| Horizontal resolution (grid size) | $\Delta x=10\text{km}$ (361 \times 289) , Lambert conformal |
| Vertical levels | 40 levels, $\Delta z=40\text{-}1180$ m |
| Initial condition for control run | JMA operational Mesoscale 4D-Var analysis |
| Breeding cycle | 12 hours (12 cycles) |
| Lateral boundary condition | JMA operational Regional model 3 hourly (no perturbation) |
| Dynamics | HE-VI scheme, $\Delta t=40$ sec, $\Delta \tau=11.4$ sec |
| Cloud microphysics | 3 ice bulk method |
| Convective parameterization | Modified Kain-Fritsch scheme |
| Turbulence | Diagnostic TKE |
| Ground temperature | Prognostic 4 soil levels, (no initial perturbations) |

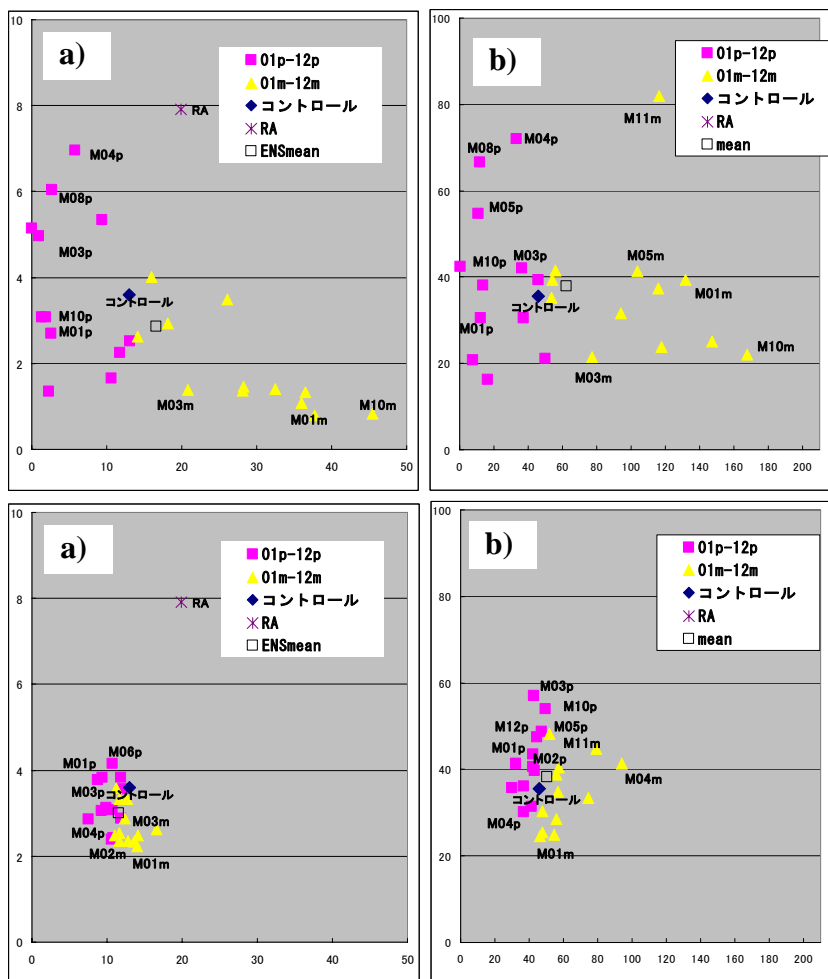


Fig. 2. Same as in Fig. 1. In case initial perturbations are given by the BGM method.

Fig. 1. a) Averaged 6 hour accumulated rain over northern Japan (rectangle in Fig. 3). Horizontal axis is for FT=00-06, while vertical axis is for FT=12-18. b) Same as in a), but for maximum rainfall amount. Initial time is 12 UTC 12 July 2004. In case initial conditions are given by Meso 4D-Var with normalized perturbations by the Global EPS.

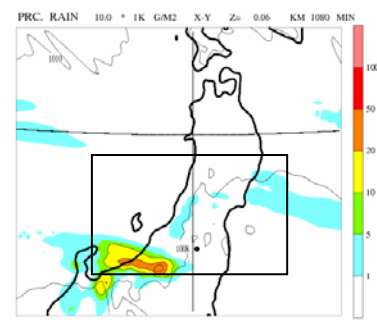


Fig. 3. Simulated 3 hour rainfall of member 'M03p' at FT=18. Initial perturbation is given by the BGM method.

References

- Saito, K. M. Kyouda and M. Yamaguchi, 2006a: Mesoscale Ensemble Prediction Experiment of a Heavy Rain Event with the JMA Mesoscale Model. *CAS/JSC WGNE Research Activities in Atmospheric and Oceanic Modelling*, **36**, 5.49-5.50.
- Saito, K., T. Fujita, Y. Yamada, J. Ishida, Y. Kumagai, K. Aranami, S. Ohmori, R. Nagasawa, S. Tanaka, C. Muroi, T. Kato and H. Eito, 2006b: The operational JMA nonhydrostatic mesoscale model. *Mon. Wea. Rev.*, **134**, 1266-1298.

Verification method to evaluate simultaneously both intensity and coverage of precipitation forecast

Tomonori Segawa and Yuki Honda

Numerical Prediction Division, Japan Meteorological Agency; 1-3-4 Otemachi, Chiyoda-ku, Tokyo 100-8122, Japan

E-mail: t-segawa@met.kishou.go.jp, honda.yuuki@met.kishou.go.jp

1. Introduction

The Japan Meteorological Agency (JMA) has been operating a mesoscale numerical weather prediction system (hereafter MSM) since March 2006 using the JMA non-hydrostatic model with a horizontal grid spacing of 5 km. The forecast time of MSM is planned to be extended from 15 up to 33 hours for 4 times a day from May 2007 (hereafter MSM0705) (Hara et al. 2007). In order to evaluate the performance of MSM0705, verifications were carried out with a new method which could assess simultaneously both the intensity and the coverage of precipitation forecasts.

2. Problems in verification for high-resolution precipitation forecasts

The accuracy of MSM against “Radar-Rain gauge Analyzed Precipitation” (hereafter R-A) has been gradually improved since March 2001, although it has been changed monthly (JMA 2007). According to the subjective verification of MSM0705, the precipitation forecasts became very realistic. However, the statistical verification score of binary categorical forecast by MSM0705 is sometimes poorer than that by the regional spectral model of JMA (hereafter RSM) using a horizontal grid spacing of 20 km (Fig.1). The details of verification are shown in Table 1.

Figure 2 gives schematic diagrams to show distinctions of scores between 10-km model and 5-km model. When the green grids are noticed, it is evident that the forecast result of 5-km model is more realistic than that of 10-km model. On the other hand, the threat score of 5-km model is poorer than that of 10-km model because the number of false alarm grids by 5-km model are larger in number than that by 10-km model (Fig.2(e) and (f)).

This discrepancy comes from the fact that the threat score using a precipitation data averaged over a verification grid is inappropriate to the verification of high-resolution precipitation forecasts. This is because the process of averaging smoothes out the peak of the grid value of precipitation which might be represented better in the high-resolution model. So, the benefit of high-resolution model would be lost if the model is evaluated by the threat score. Therefore, it is necessary that both the intensity and the coverage of precipitation forecasts are assessed at the same

time.

3. Precipitation Area Score

The precipitation area score (PAS) is defined as

$$PAS = \frac{1}{N} \sum_{i=1}^N (RPf_i - RPo_i)^2,$$

where

RPf (or RPo): Ratio of forecasted (or observed) precipitation area over the threshold in a verification grid.

N: Total number of verification grids in target domain. This article covers PAS in one verification grid where both RPf and RPo are zero is not calculated like the threat score.

The characteristics of PAS are shown as follows:

- (1) It has a range of 0 to 1, 0 for a perfect forecast.
- (2) It is tolerant of the position error of forecast and observation within a verification grid. If $RPf = RPo$ in one verification grid, PAS of this grid is zero.
- (3) It is designed to assess both the intensity and the coverage of precipitation forecasts at the same time.
- (4) The score can evaluate high-resolution forecasts without the process of averaging which smoothes out the peak of the grid value of precipitation.
- (5) It is possible to evaluate both high-resolution and low-resolution deterministic forecasts simultaneously by taking a verification grid as the lower-resolution model grid.

The results of verifications using Fig.2(a)-(c) are shown in Fig.2(f). It becomes evident that PAS of 5-km model is better than 10-km model, even if threat scores of 5-km model are poorer than that of 10-km model. Thus, PAS makes the disagreement small between the subjective verification and the objective verification.

4. Examination of verification of MSM0705 and RSM using PAS

As shown in Fig.3, the results of verification using PAS are shown as follows:

- (1) MSM0705 is obviously superior to RSM for the 1mm/3h and 10mm/3h precipitation forecasts. Even if the forecast time is longer, the rate of the deterioration of MSM0705 is slower than that of RSM. This result is contrary to one derived from the threat score (Fig.1).
- (2) MSM0705 is still better than RSM for even 30mm/3h precipitation forecasts. As shown in

Fig.4, the forecasted precipitation area and the observed precipitation area by R-A which are arranged initial times of MSM0705 are nearly equal. On the other hand, the forecast area of RSM is smaller than the observed one. Thus, judging from these results, it is considered that non-forecasting is better than forecasting somewhere in the case of heavy rainfall.

(3) As the threshold becomes larger, PAS decreases on the whole. However, this does not mean the accuracy of precipitation forecasts for heavy rainfall is higher, but that the differences between RPF and RPo of rare events are generally smaller.

5. Concluding remarks

PAS makes the disagreement small between the subjective verification and the objective verification, when the objective verification of high-resolution forecast is worse than that of low-resolution forecast although the high-resolution forecast is more realistic than the low-resolution one.

PAS of MSM0705 is better than that of RSM against all thresholds and forecast time, even if threat score of MSM0705 is poorer than that of RSM.

The formulation of PAS is very similar to that of "Brier Score". Thus, it will be possible to compare the low-resolution probabilistic forecasts and the high-resolution deterministic forecasts using a lower-resolution verification grid at the same time.

References

Hara, T. et al., 2007: Upgrade of the operational JMA non-hydrostatic mesoscale model. *CAS/JSC WGNE Res. Act. in Atmos. and Ocea. Modelling*.
 Japan Meteorological Agency (JMA), 2007: OUTLINE OF THE OPERATIONAL NUMERICAL WEATHER PREDICTION AT THE JAPAN METEOROLOGICAL AGENCY. *Appendix to WMO Numerical Weather Prediction Progress Report*, JMA, Tokyo. 194pp.

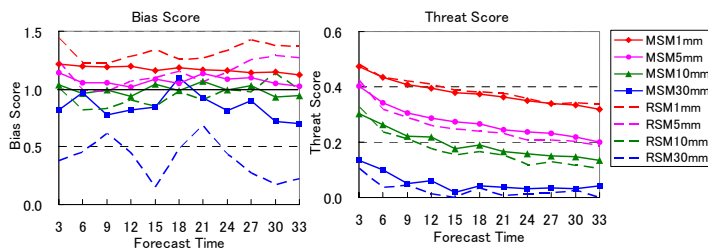


Fig.1. Time sequences of bias and threat scores by MSM0705 and RSM. "MSM1mm" denotes the score of MSM0705 for 1mm/3h.

| | MSM0705 | RSM |
|--------------------------------------|--|--------------------------|
| Verification Grid Size | 40km × 40km | |
| Amounted Time | 3 hours | |
| Initial Time | 03.09.15.21UTC | 00.12UTC |
| Forecast Time | 33 hours | |
| Threshold of Precipitation Intensity | 1, 5, 10, 30mm/3h | |
| Verification Term | Summer (31 days, from 1 July 2006) Winter (31 days, 22 Dec. 2005) | |
| Number of Initials | 248(summer) 248(winter) | 62(summer) 62(winter) |
| Verification Domain | Japan and around sea | |
| Observation Data | Radar-Raingauge Analyzed Precipitation (1-km mesh) | |

Table 1. Details of statistical verification of MSM0705.

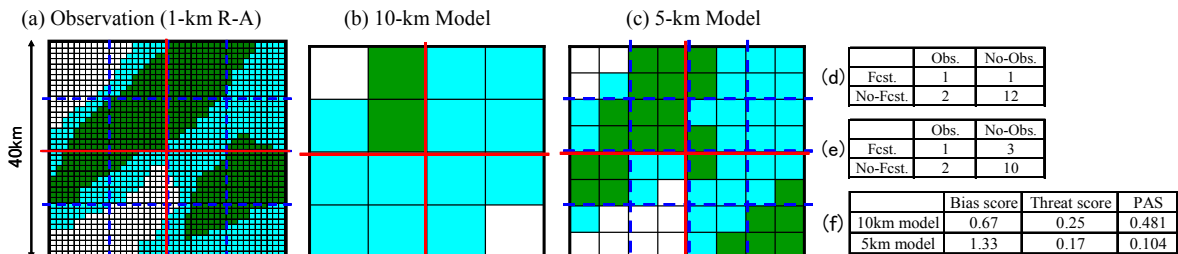


Fig. 2. Schematic diagrams to compare the threat and bias scores with PAS, contingency tables, and verification results.

The light blue area represents the precipitation intensity more than 1mm/3h, and the green area represents that of more than 5mm/3h. (a): Observation of R-A with 1-km grids. (b): Forecasts of model with 10-km grids. (c): Forecasts of model with 5-km grids. (d): The 2x2 contingency table of 10-km model with 10-km verification grid. (e): Same as in (d) but with 5-km model. Both contingency table and PAS use the threshold of 5mm/3h. Contingency tables use 10-km verification grids (blue dashed line). (f): Results of verification using contingency tables and PAS. The PAS is evaluated with 20-km verification grid (red lines).

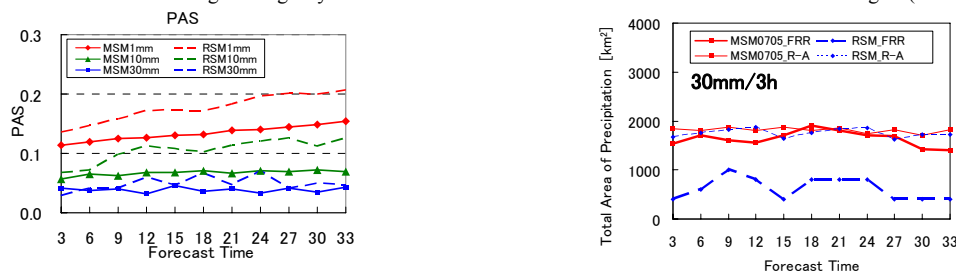


Fig.3. PAS of MSM0705 against forecast time. "MSM1mm" denotes the score of MSM0705 for 1mm/3h. The dashed lines denote PAS by RSM. The details of this verification are shown in table 1.

Fig.4. Total area of precipitation of MSM0705 against forecast time.

The red lines represent MSM0705, and the blue lines RSM. The thick lines denote total area of precipitation by MSM0705 and RSM, and the thin lines denote that by R-A. "FRR" denotes the forecasted precipitation.

Japan Area Mesoscale Ensemble Experiments using JMANHM

Hiromu Seko*, Kazuo Saito*, Masaru Kunii*
Tabito Hara**, Masayuki Kyouda** and Munehiko Yamaguchi**

* Meteorological Research Institute, Tsukuba, Ibaraki 305-0052, Japan; hseko@mri-jma.go.jp

** Numerical Prediction Division, Japan Meteorological Agency

1. Introduction Even if weather forecast is performed using perfect models, analysis error increases with time because the chaos of atmosphere increases the observation error and analysis error. Thus, the state of atmosphere should be seen as the existing probability. Ensemble forecast adds the information of the probability to the deterministic weather forecast. Moreover, the forecasts of members can reduce the risk of the undetected heavy rainfalls. Therefore, the ensemble forecast is expected to be useful for the disaster prevention. With collaborating with Japan Meteorological Agency (JMA), Meteorological Research Institute participates in the meso-scale ensemble forecast component of WWRP Beijing 2008 Forecast Demonstration / Research and Development Project (hereinafter, Beijing project). It is instructive to apply the techniques, which have been developed in the Beijing project, to other regions in order to confirm of their validity. The result of Japan area ensemble experiments using the technique developed by Saito et al. (2006) is explained in this study.

2. Specification of ensemble experiments The numerical model and the producing method of the initial perturbation were the same as those of WWRP Beijing project. The domain of the model is set to be 3000 km x 3300 km. The horizontal grid interval is 15 km. The initial perturbation was produced by adding the normalized perturbation of one-week ensemble of JMA to the initial fields of the JMA Regional Spectrum Model (RSM) (Saito et al. 2006). The period of ensemble experiment is from 8 to 20 August of 2006, which is around the same time of the Beijing project. Numerical predictions of 11 members were performed from the initial time of 21 JST. Figure 1 shows the examples of the forecast. On 18 August, typhoon 0610 passed the southern part of Japan. The intense rainfalls occurred near the typhoon and along the Pacific side. Results of ensemble experiments were evaluated by comparing 2m temperature and 3hour accumulated rainfall with the observation data of Automated Data Acquisition System of JMA.

3. Results of ensemble experiments Figure 2 shows the comparison of easterly wind at 24hour forecast between the control run and the ensemble mean. The control run is the forecast from the initial condition without initial disturbances. Namely, the initial condition of control run was produced by the interpolation of RSM outputs. These forecasts were compared with the next day's initial fields of which the valid time is the same as 24hour-forecasts. Error of the ensemble mean was smaller than those of the control run (fig. 2). The ensemble mean of other forecast variables, e.g. southerly wind and temperature, are also smaller than those of control runs. This feature was also recognized in Beijing project (fig. 3 in Saito et al. in this volume). The error of Japan area experiment (Japan case) was larger than those of Beijing project, because the typhoons 0607 and 0610 passed the Japan during the ensemble experiment period. Figure 3 shows the temporal variation of ensemble spreads. The spreads of surface pressure and horizontal wind had increased during the forecast period (36 hour). On the other hand, the spreads in Beijing project stopped increasing at about 27 hour (fig. 4 in Saito et al. in this volume). This difference was produced by the relative position of verification area to the boundary. The verification area of the Japan case is located at more inside of the simulation domain. Then, the influence of boundary, which did not contain the perturbation in this experiment, became weaker than that in the Beijing project. Diurnal variation is clearly seen in temperature, relative humidity and precipitation. However, the diurnal variation of temperature is much smaller than that of Beijing project, because the ocean occupies the large area of the experiment domain. Figure 4 shows the bias score of 3hour accumulated rainfall in the control run and ensemble mean. When the threshold value is 0.1 mm, the bias score of ensemble mean is much larger than that of the control run because of the expansion of the weak rainfall region. When the threshold is larger than 2 mm, there is no large difference in both scores. The threat score was also compared with the threshold of 3 mm, where the bias score is close to 1. The score of ensemble mean is larger than the control run, except 0.1 mm (fig. 5). These scores mean that the ensemble mean is closer to the observation. This comparison indicates the usefulness of the ensemble forecast.

4. Summary The technique developed in Beijing project is useful for the prediction. The technique, which will be developed in Beijing project, will be checked using Japan area experiments to confirm its validity.

References

Saito, K. M. Kyouda and M. Yamaguchi, 2006: Mesoscale Ensemble Prediction Experiment of a Heavy Rain Event with the JMA Mesoscale Model. CAS/JSC WGNE Research Activities in Atmospheric and Oceanic Modelling. **36**, 5.49-5.50.

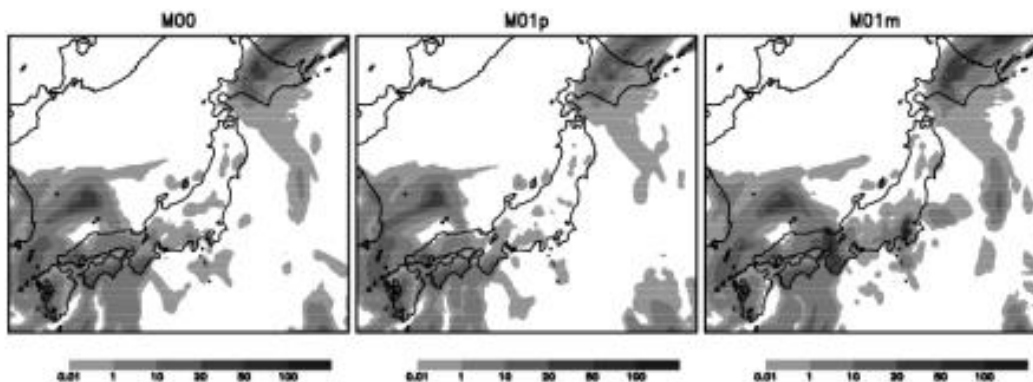


Fig. 1. 3 hour accumulated rain for 6 hour forecast of JMA-NHM with the control run (Left), member M01p (center), and member M01m (Right). Initial time is 21 JST 18 August 2006.

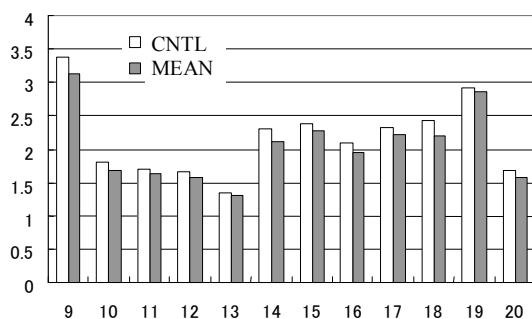


Fig. 2. 24 hour forecast RMSEs of the control run and the ensemble mean against initial condition over the verification domain. Verification period is 12 days from 8 to 20 August.

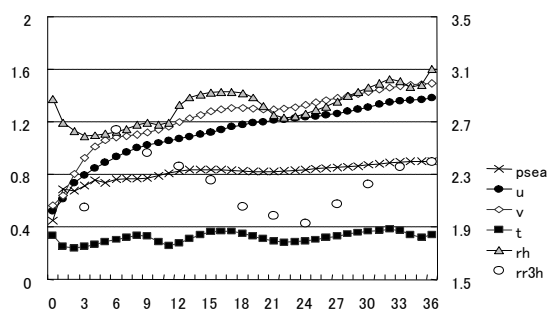


Fig. 3. Time sequences of the ensemble spreads. Unit of the left vertical axis is 'hPa' for MSL pressure (PSEA), 'm/s' for horizontal winds (U and V), 'K' for 2m temperature (T), respectively. Unit of the right vertical axis is '%' for relative humidity (RH) and 'mm' for 3 hour accumulated rain (RR3H), respectively.

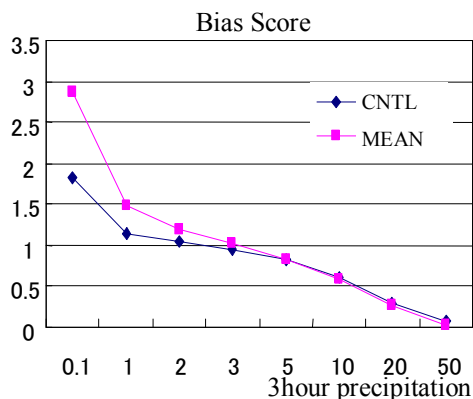


Fig. 4. Bias score of the control run and the ensemble mean. Verification period is 12 days from 8 to 20 August.

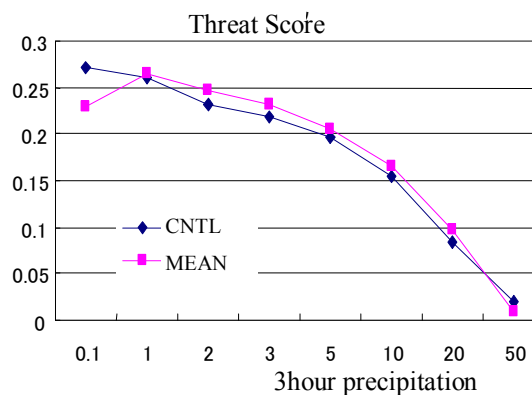


Fig. 5. Threat score of the control run and the ensemble mean with threshold of 3mm. Verification period is 12 days from 8 to 20 August.

Advanced Model of Atmospheric Boundary Layer

V. Shnaydman (volf@envsci.rutgers.edu) and G. Stenchikov
Rutgers University, New Brunswick, NJ

L. Berkovitch

Russian Hydro-meteorological Research Centre, Moscow

In this study an advanced turbulent closure scheme is used to improve simulation of 3-dimensional distribution of meteorological variables and turbulence characteristics in atmospheric boundary layer (ABL). It included two transport equations for turbulent kinetic energy and dissipation rate [Shnaydman and Berkovitch, 2006]. This closure scheme is superior with respect to the Mellor-Yamada closure. Similar schemes are used in the advanced computational fluid dynamics codes like FLUENT [Huber *et al.*, 2004; Lesieur, *et al.*, 2002]. The advanced ABL model explicitly describes effect of large eddies. Medium range anisotropic eddies are handled by Smagorinsky model, and effect of small inertial-range eddies is calculated using two-equation closure parameterization of Shnaydman, [2004].

The advanced ABL model has been coupled with the hemispheric forecast model of the Russian Hydrometeorological Center [Shnaydman and Berkovitch, 2006]. The results were obtained for the meteorological conditions of the USA, Canada (20-55°N, 70-125°W), and Europe, Central Russia. The calculation period was 36 hours with initial time 00:00 UTC April 12, 2005. Here we conduct a detailed analysis of vertical distribution of meteorological variables and turbulence parameters.

The most intensive turbulent exchange was obtained for noon hours. The dominant mechanism of the turbulent mixing was the strong non-stable thermal stratification. The intensive turbulent exchange restricted vertical gradient of horizontal wind in the layer from 100 m till the ABL top of 1200 m. Under these conditions the maximal values of turbulence coefficient (K_z), turbulent kinetic energy (TKE) and dissipation rate ϵ reached, respectively $65 \text{ m}^2/\text{s}$ (at $z=300\text{m}$), $2.3\text{m}^2/\text{s}^2$ (at $z= 100\text{m}$), and $0.06 \text{ m}^2/\text{s}^3$ (in roughness layer). By using the values of TKE and ϵ in the Kolmogorov-Prandtl relationship the vertical length (L) and time (τ) scales could be calculated. The maximal spatial and temporal scales were equal to 47 m and 332 s, respectively. This value of turbulence length scale corresponds to the inertial interval of the TKE spectrum. The product of time scale to the speed of horizontal motions gave a horizontal length equals approximately to 5 km. The vertical length calculated using speed of organized vertical motions appeared to be about 100 m. The associated anisotropy coefficient of 0.02 in the boundary layer is two times larger than in the free atmosphere.

The weakest turbulent exchange was found for night hours. The forcing mechanism of the turbulent mixing for these conditions was interaction of stable stratification and turbulent exchange. The ABL top was at 300 m only. The maximal values of K_z , TKE and ϵ were $8.0 \text{ m}^2/\text{s}$, $0.96 \text{ m}^2/\text{s}^2$ and $0.012\text{m}^2/\text{s}^3$, respectively. The maximal length and time scales were 12 m and 125 s, respectively. Vertical and horizontal lengths were 2 km and 30 m, and the anisotropy coefficient was about 0.015.

Mean values of turbulence characteristics and their limits under different meteorological conditions were calculated for different temperatures and wind stratifications. The typical ABL turbulence parameters for selected ranges of vertical temperature gradient and wind shear are given in the tables 1, and 2.

Table 1. Typical ABL parameters for selected ranges of vertical temperature gradient

| Stratification n deg/100m | K_z m^2/s | L m | Limits Kz L | TKE m^2/s^2 | τ s | Limits TKE τ |
|---------------------------------|------------------|--------|---------------------|------------------|-------------|----------------------|
| < - 2.0 | 41 | 33 | 31-65 31-48 | 1.8 | 228 | 1.0-3.2 250-310 |
| -2.0 --- -1.0 | 28 | 24 | 21-43 23-27 | 1.4 | 200 | 0.8-2.5 172-262 |
| - 1.0 --- 0.0 | 13 | 15 | 6-20 9-18 | 0.6 | 185 | 0.4-0.8 150-250 |
| > 0.0 | 5 | 9 | 1-12 3-10 | 0.3 | 167 | 0.1-0.4 100-200 |

Table 2. Typical ABL parameters for selected ranges of wind shear

| Stratification n m/s per 100m | K_z m^2/s | L m | Limits Kz L | TKE m^2/s^2 | τ s | Limits TKE τ |
|--|------------------|--------|---------------------|------------------|-------------|----------------------|
| > 2.0 | 30 | 20 | 20-43 17-24 | 2.1 | 143 | 1.4-3.2 134-176 |
| 2.0 --- 1.0 | 9 | 10 | 5-22 6-17 | 0.9 | 100 | 0.6-1.6 83-137 |

The predicted ABL internal structure calculated within the forecast model was tested against the ABL adapted to the characteristics of the free atmosphere obtained from operational objective analysis. The simulated driving characteristics in the 24 hours forecast at the bottom and at the top of ABL were in good agreement with the operational objective analysis. The predicted values inside the ABL agreed with adapted parameters which were obtained from the stationary solution of the closed system of hydrodynamic and closure scheme equations and the objective analysis fields as the boundary conditions. The predicted and adapted variables had similar vertical distributions and differences in wind magnitude and direction were 0.8 m/s and 12-18°. The differences in vertical temperature gradients were 0.2-0.3° per 100m. Thus, the relative error in simulated turbulent parameters did not exceed 20%.

We found that the developed model eliminates the main shortcomings of Mellor-Yamada description of ABL internal structure. It is more physically consistent because it simultaneously accounts for the impacts of large, intermediated and small eddies, and describes the locally isotropic sub-grid turbulence. The results of application in the Russian Hydro-meteorological Research Centre operational forecasting reveal the effectiveness of ABL modeling and downscaling in the numerical prediction operations.

References

- Huber, A., Tang, W., Flowe, A., Bell, B., Kuehlert, K., and Schwarz, W., 2004: Development and Applications of CFD Simulations in Support of Air Quality Studies Involving Buildings. Preprints, 13th Joint Conference on the Applications of Air Pollution Meteorology, US EPA.
- Lesieur, M., Metais, O., Compte, P., 2002: Large-Eddy Simulations in Turbulence, Cambridge U. Press, New York, 219pp
- Shnaydman, V., 2004: Improved Hydrodynamical Scheme of Turbulence Description, Research Activity in Atmospheric and Oceanic Modeling, No 34, and 4.29-4.30.
- Shnaydman, V., Berkovitch, L., 2006: Atmospheric Boundary Layer Modeling in the Numerical Prediction Operations, Research Activity in Atmospheric and Oceanic Modeling, No 36, 5.57-5.57

Improvement of photochemical oxidant information by applying transport model to oxidant forecast

Isao Takano, Yuri Aikawa and Susumu Gotoh

Japan Meteorological Agency

E-mail: itakano@met.kishou.go.jp, aikawa@met.kishou.go.jp

1. Introduction

The Japan Meteorological Agency (JMA) has produced a statistical guidance of oxidant using weather and pollutant observation and issued photochemical oxidant information for prefectures in high oxidant concentration days.

To offer more detailed information in time and in space, we have developed an atmospheric transport model that takes in the forecast of the operational mesoscale NWP model (MSM) and the air pollutant observation.

The statistical verification showed that the information produced by the atmospheric transport model was more accurate than that by the statistical guidance.

2. Methodology

The JMA obtains air-pollution observation in the southern part of the Kanto region using private lines from the Tokyo metropolitan Government immediately, and those in northern part of the Kanto region through internet from the website AEROS¹ within two hours. Analysis of oxidant concentration at 03UTC is calculated as a weighted average of observation data at each horizontal grid with a spacing of 0.1 degree in lat. 35-37°N and long. 139-141°E.

High oxidant condition is produced through complex photochemical processes involving NO₂ and other gases. We approximated oxidant production during the forecast period using NO₂ concentration and model-forecast solar radiation and temperature.

Assuming that the time tendency of the NO₂ concentration is small, NO₂ concentration at 03UTC is applied to 03-08UTC. This estimated oxidant concentration is proportional to NO₂ concentration using a coefficient dependent on solar radiation and surface temperature of MSM outputs.

The atmospheric transport model (Iwasaki et

al., 1998; JMA, 2002) is applied to oxidant forecast. One hundred thousand particles are released at the analysis time and the location (distributed uniformly 0-500m above ground here) and transported with a time interval of 10 minutes using the hourly outputs of MSM at 00UTC initial time. The dropped and deposition schemes are not used. The horizontal diffusion scheme depends on Gifford (1982). It adopts Gifford (1977), which treats a similar time scale, as a diffusion parameter. Some particles are emitted after 04UTC as oxidant generated from NO₂.

3. Verification Experiments and results

The performance of the statistical guidance and the atmospheric transport model are compared with cases of 9 days in August 2006 that the photochemical oxidant information was announced and the oxidant concentration reached to the level of the photochemical oxidant advisory (120ppb).

If both the analysis and the forecast include (or do not include) a high oxidant concentration grid within a first subdivision forecast district (where a prefecture is divided into several), it is assumed to be a hit, and a failure when only the forecast includes a high concentration grid, and a miss when only the analysis includes a high concentration grid.

The maps of the oxidant concentration of the analysis and the five-hour forecast at 08UTC on 4 August 2006 are shown in Fig. 1. A high concentration region of the forecast captures that of the analysis very well.

The hourly scores of the model and the guidance at 04-09UTC for 9 days in the southern part of the Kanto region is shown in Fig. 2. The hit rate of model exceeds that of the guidance throughout the forecast time. Besides, the false rate of the model is equal to and the missing rate is less than those of the guidance.

¹ Atmospheric Environmental Regional Observation System, <http://soramame.taiki.go.jp>

4. Conclusion

The result indicates that the transport model applied to the oxidant contributes to the improvement of the forecast. In addition, the model has good precision in each forecast district throughout the forecast time in the southern part of the Kanto region. The JMA comes to be able to announce the photochemical oxidant information supplemented with the model oxidant forecast 04-09UTC in this area after 04UTC.

On the other hand, there is some difficulty in the forecast of high oxidant concentration areas in the northern part of Kanto, which is mostly attributable to the discrepancy of the analysis time and the observation time there.

MSM plans to adopt a hybrid terrain following vertical coordinate (JMA, 2007), then the transport model will be modified to adopt the same coordinate.

References

- Gifford, F. A., 1977: Tropospheric Relative Diffusion Observations. *J. Appl. Met.*, **16**, 311-313
- Gifford, F. A., 1982: Horizontal diffusion in the atmosphere: A Lagrangian-dynamical theory. *Atmos. Environ.*, **16**, 505-512
- Iwasaki, T., T. Maki, and K. Katayama, 1998: Tracer transport model at Japan Meteorological Agency and its application to the ETEX data. *JMA/NPD Tech. Rep.*, **35**, 4285-4295
- JMA, 2002: Outline of operational numerical weather prediction at Japan Meteorological Agency. Available from Numerical Prediction Division, JMA. 158pp
- JMA, 2007: Outline of operational numerical weather prediction at Japan Meteorological Agency. Available from Numerical Prediction Division, JMA. 197pp

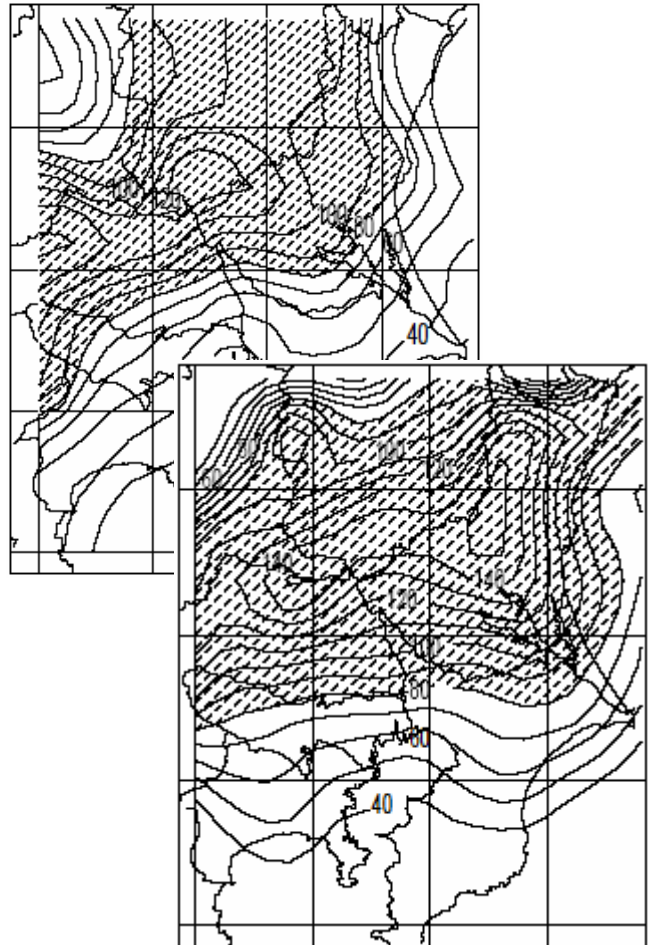


Fig. 1 The oxidant concentration of the analysis and the forecast at 08UTC Aug 4th 2006 (upper chart: analysis, lower chart: forecast). The area exceeding 80ppb is hatched.

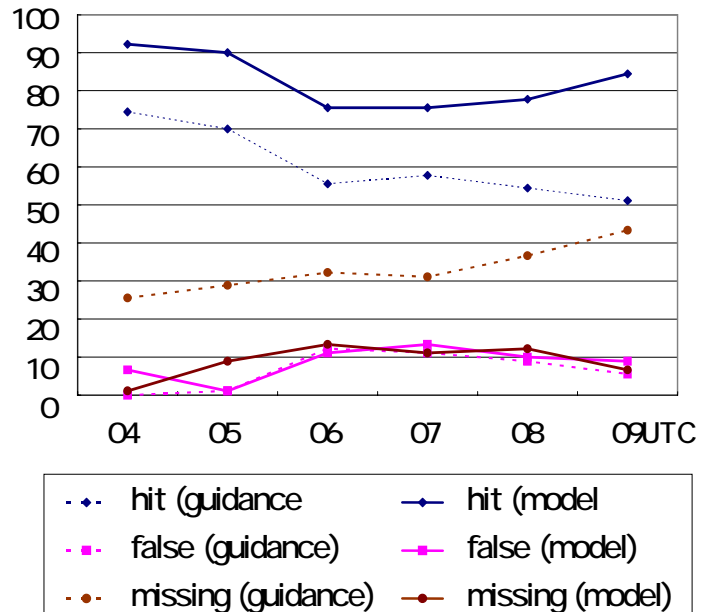


Fig. 2 The hourly scores of model and guidance between 04UTC and 09UTC for the 9 days in the southern part of Kanto.

Installation of the Unified Model for NWP in South Africa

Warren Tennant (warren.tennant@weathersa.co.za)

South African Weather Service (SAWS)

Introduction

The South African Weather Service (SAWS) installed the Met Office Unified Model in 2006. This modelling system was selected to become the SAWS operational in-house numerical weather prediction (NWP) model for forecast guidance up to two days ahead from December 2006.

The SAWS has maintained an operational NWP system with data assimilation (DA) since 1993. This first system was based on the National Centers for Environmental Prediction (NCEP) regional Eta model. Table 1 shows the model resolution and forecast statistics for this period. Performance of this system improved steadily in sync with increasing computer capacity and improved model skill, roughly equivalent to a doubling of forecast lead-time for the same level of skill over the decade. The UM forecasts (last line) show a greatly improved skill using these same metrics but results are as yet only available for a relatively short period.

Table 1: Average statistics for 12-month periods for SAWS Eta forecasts

| RMS Error | | 24-h | | 48-h | |
|---------------|--------------|------------|------------|------------|------------|
| Model version | Dates | MSLP (hPa) | 500Z (dam) | MSLP (hPa) | 500Z (dam) |
| Eta80km17L | 1994-1995 | 2.508 | 2.079 | 3.721 | 3.631 |
| Eta80km38L | 1996-1997 | 2.042 | 1.959 | 3.434 | 3.437 |
| Eta48km38L | 1998-1999 | 1.813 | 1.755 | 2.576 | 2.550 |
| Eta48km38L | 2000-2001 | 1.810 | 1.548 | 2.467 | 2.432 |
| Eta48km38L | 2001-2002 | 1.755 | 1.489 | 2.474 | 2.415 |
| Eta32km45L | 2002-2003 | 1.519 | 1.387 | 2.181 | 2.182 |
| UMSA12km38L | Nov06-Feb07* | 0.995 | 0.714 | 1.454 | 1.080 |

* UM verification is only available for a short period during the austral summer, but the Eta32km45L and UMSA12km38 domains are very similar in size and location

Operational UM Configuration at the SAWS

The South African domain of the UM was chosen to be similar in size to the Met Office NAE12km, and covers all of southern Africa south of the equator to 45°S, and 10°W to 60°E. The horizontal resolution was set at 12km with the standard set of 38 levels in the vertical, as used at the Met Office. This domain is intended to form the basis for the provision of initial dumps and lateral boundary conditions (LBCs) to other centres in the region who wish to run limited area versions of the UM in this domain, thus lifting the pressure on the Met Office to fulfil this role.

The UM system at the SAWS runs a full 3D-VAR data assimilation system, but tests on a 4D-VAR upgrade are also being done. The Met Office provides an intermediate observation file every six hours on the SAWS SA12 domain that is transferred to the SAWS in real time, thus eliminating the need to interface the Observation Processing System (OPS) with a local

observation database. Historically this has been a weak point in the SAWS NWP system. Justification for running a data assimilation cycle at the SAWS is based on the findings of an earlier study with the Eta 32km45L model where a clear degradation in the forecast skill at 24 and 48 hours was apparent when data assimilation was switched off. Furthermore, the finer resolution SA12 model can exploit more of the high-density satellite data than the relatively coarser UM global model.

Research Applications using the UM

Preliminary research work started at the SAWS includes case studies to investigate the model simulation of rainfall over the summer rainfall region of South Africa at 15km resolution plus successive nests within that domain of 5km and 1.7km respectively. The aim of this experiment was to determine whether the UM can improve upon the spatial distribution of convective-type rainfall as horizontal resolution increases. Convective parametrization is switched off for the 1.7km run based on the assumption that convective processes are resolved at this horizontal resolution. Five case studies were chosen between March and August 2006 to cover varying synoptic situations and seasons. Results for the case of 22 April 2006 is shown in figure 1. The plotted areas roughly depict the model domains. It becomes clear that the 5km and 1.7km resolutions capture the RADAR observed streak pattern in rainfall, while the 15km does not. The topographical influence on rainfall is best captured at the 1.7km resolution, as seen toward the upper part of the figure where mountain ranges are present. These early results indicate that resolutions less than 5km ought to be quite successful in capturing the spatial structure convective rainfall at least in a qualitative sense. Clearly it would be short-sighted to expect the model to place these events correctly unless topography plays the only dominant role in convective development during a particular event.

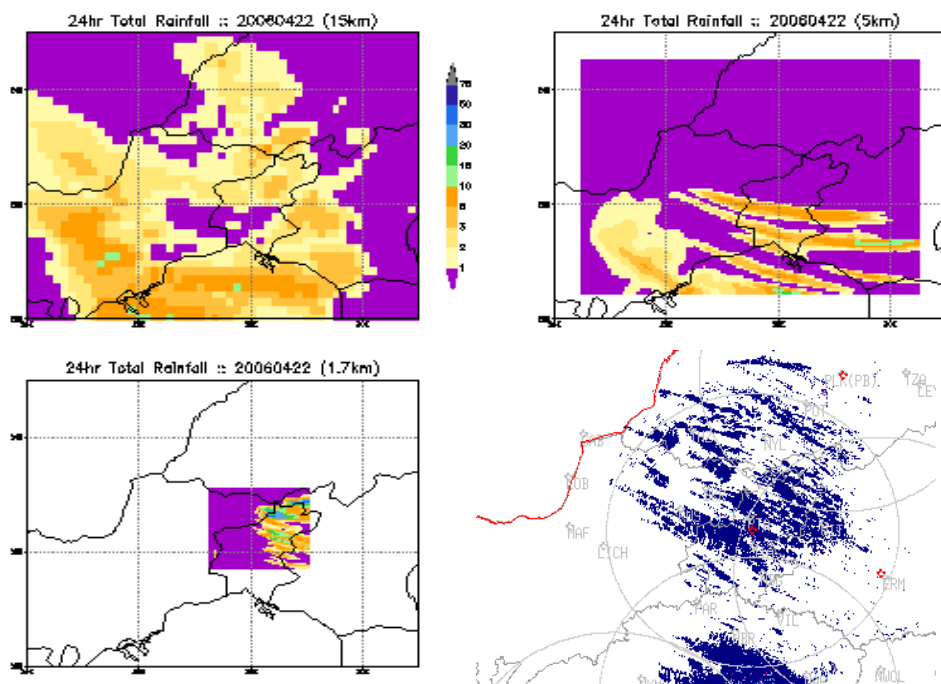


Fig. 1: Total 24-hour forecast precipitation for 22 April 2006 (0-hour lead time) simulated by the UM at 15km (top left), 5km (top right) and 1.7km (bottom left), and radar rainfall estimates (bottom right).

Seasonal Prediction at the Regional Scale: An Analysis of Regional Climate Model Performance Over the Tropical Americas.

Etienne TOURIGNY, Colin JONES

Université du Québec à Montréal – CRCMD Network, Canada
tourigny@sca.uqam.ca

1. Introduction

The main goals of seasonal prediction are to forecast climatic variables of societal interest over 3 to 9 month lead times in order to alleviate the potential consequences of climatic extremes and to assist in resource planning in fields such as agriculture. The drawback of current global scale seasonal forecasting is their low resolution. Regional models can be used to produce more useful forecasts through their higher resolution response to global phenomena. In tropical regions, large-scale atmospheric circulations are linked to the more slowly evolving Sea Surface Temperatures (SST). Anomalous SST forcing such as ENSO drives large scale atmospheric anomalies which have consequences on the regional scale.

In order to assess the added value of regional scale models in seasonal forecasting, the output of hindcasts using these models must be evaluated and compared to observations. Using prescribed SST and analysed lateral boundary conditions, the Rossby Center Regional Climate Atmospheric Model RCA3 (Jones 2004), has been used to make high resolution simulations. Emphasis is put on El Niño and La Niña composites and the comparison of the model to observations. This will determine if RCMs, when given accurate large-scale forcing, are able to reproduce the main regional scale climatic features over the tropical Americas and the detailed response in this region to the phase of ENSO. The study looks at interannual variability associated with ENSO at two time scales: seasonal and sub-seasonal (using pentad values).

2. Numerical Experiment

The Rossby Center Regional Atmospheric Model RCA3 was run over Central America with a resolution of 0.33° (~37km) and grid size of 276x168 using observed SST and ECMWF ERA40 reanalyses for initial and boundary conditions. The simulations were of 13 months each (1 month discarded for spinup) from 1970-2005. Figure 1 shows the model domain (the outer 15 points are removed in this figure and are not included in any analysis) and the regions chosen for analysis. We present here only results for the CAM (Central America) region.

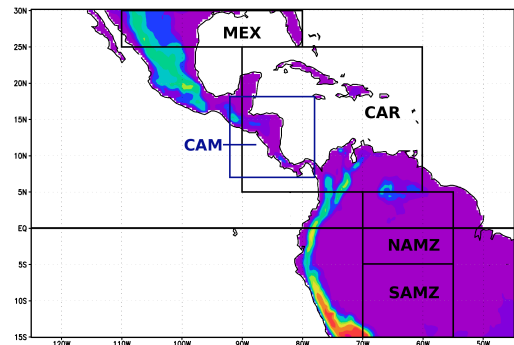


Fig. 1 Domain of the study and chosen regions

3. Results for seasonal timescale

Figure 2 shows the climatological average of monthly means of precipitation for years 1979-2001. for the CAM region. The model (RCA) is compared to GPCP (GPCPv2, satellite), CRU (land-based) and ERA40. The model values are comparable to GPCP but lower than CRU. ERA40 data is much too wet to be used as an observation over this region.

The technique used to evaluate the ability of the RCM to simulate inter-annual variability due to ENSO is to compute the differences of El Niño and La Niña composites normalized by climatology. This is done to ensure that any bias in the model's climatology is removed from the ENSO results. Composites span two years (0 and +1) representing mean conditions in the two years of ENSO events. Figure 3 shows the result of ENSO difference over CAM region. The model follows the general tendencies in the observations, but shows excessive drying from APR-SEP of year(0). The most documented period of dryness in El Niño years is JUL-OCT of year(0) (Ropelewski 1987), and in this period the model is in accordance with the observations although of greater magnitude.

4. Results for sub-seasonal timescale

The sub-seasonal distribution of precipitation (and its anomalous distribution in ENSO years) is at least as important as the seasonal mean (and anomaly) for decision makers. Sub-seasonal timescale statistics can also indicate if the model is producing precipitation in the right way. We examine the frequency distribution of precipitation during the rainy season divided into intensity bins. The

model is compared to GPGP pentad (GPCP), over the 1979-2003 period.

Figure 4 shows the climatological distribution for the CAM region. The way this is done is to compute the distribution for each grid point for each rainy season, followed by a spatial average over the area and temporal average over the analysis period. The model follows rather closely the observations (with small differences) and the maxima are in the same category (5-10 mm/day). Figure 5 shows the average difference between El Niño and La Niña years. Both in observations and model, El Niño years have more frequent dryer days and less frequent wetter days than La Niña years. This is both true in the extreme (0-1, 20+) and in moderate categories. Again the differences between model and observations are quite small, with similar phase shifts in the distribution.

5. Discussion and conclusion

The Regional Climate Model RCA3 has been used to assess the ability of regional climate models to simulate seasonal and sub-seasonal anomalies associated with ENSO. In the area presented here (CAM) the model has shown to reproduce the (monthly averaged) dry conditions associated with El Niño, although the signal is more intense than in observations. When looking at the sub-seasonal distribution the model agrees quite well in simulating more dry days and less wet days in El Niño years. We believe that these positive results indicate that Regional Climate Models can be used to provide locally enhanced detail, with respect to ENSO forced seasonal variability, when run forced by global seasonal forecasts.

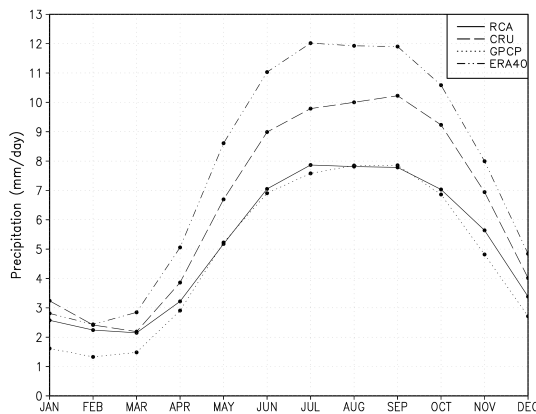


Fig. 2 Climatology over CAM region.

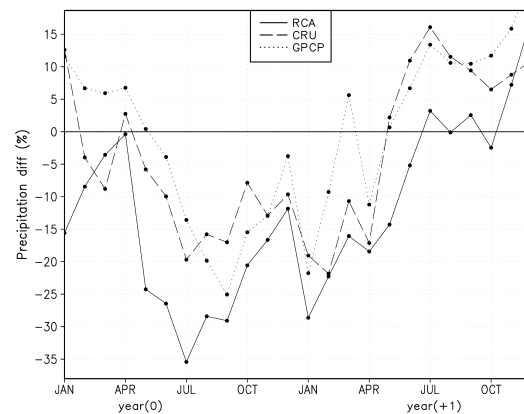


Fig. 3 ENSO differences over CAM region.

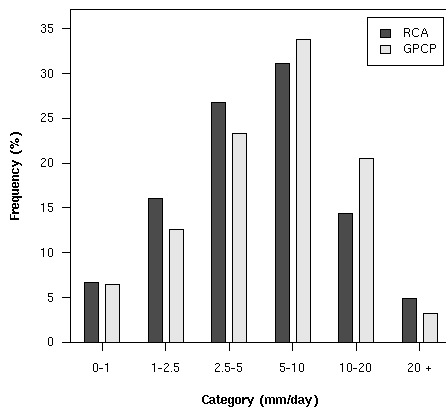


Fig. 4 Frequency distribution over CAM region.

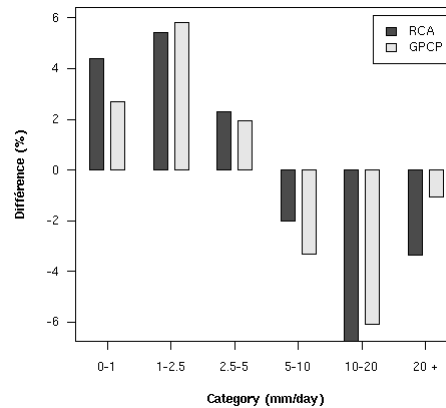


Fig. 5 ENSO differences of frequency distribution over CAM region.

References

Jones, C.G., A. Ullerstig, U. Willen and U. Hansson, 2004: The Rossby Centre regional atmospheric climate model (RCA). Part I: Model climatology and performance characteristics for present climate over Europe. *Ambio*, **33**, 199-210.
 Ropelewski, C.F., and M. S. Halpert, 1987: Global and Regional Scale Precipitation Patterns Associated with the El Niño/Southern Oscillation. *Monthly Weather Review*, **115**, 1606-1626.